A Harmonic Compensation System With Embedded Load Observer for Micro-Grids in the Islanded Mode of Operation

Sajjad Makhdoomi Kaviri, *Member, IEEE*, Majid Pahlevani, *Senior Member, IEEE*, Praveen K. Jain, *Fellow, IEEE*, and Alireza Bakhshai, *Senior Member, IEEE*

***Abstract*—This paper presents a new harmonic compensation system along with a hybrid load observer used for micro-grids in the islanded mode. The proposed control system includes an online hybrid load observer, which is able to precisely estimate the harmonic contents of the load as well as the equivalent load impedance in the islanded mode. One of the main features of the proposed control system is its capability to deal with unknown load harmonics, which is a big challenge in micro-grids. Basically, the proposed control system is able to detect, estimate, and compensate various load disturbances and harmonics (e.g., synchronous and asynchronous harmonics, and dc components). Theoretical analysis, simulation results, and experimental results verify the feasibility and performance of the proposed control system.**

***Index Terms*—Distributed generation (DG), grid equivalent impedance, harmonic compensation, islanded mode of operation, micro-grids (MGs), state observers.**

I. Introduction

DUE to substantial advantages of distributed generation (DG) over the conventional centralized power generation, DG has recently been a very active research area [1], [2]. In particular, integrating renewable energy sources (RESs) into the current power system through a DG platform has been of great interest [3], [4]. Micro-grids (MGs) are the main building blocks in the DG that can integrate RESs to the grid very efficiently [5]–[7]. The MGs must be able to operate in both the grid-connected mode (i.e., on-grid) and the islanded mode (i.e., off-grid). There are various challenges in order to provide reliable operation of MGs particularly in the islanded mode of operation [8]–[10]. In the islanded mode, the MG must be able to provide power balance and supply load currents, which can include various harmonics and disturbances. Otherwise, the voltage will be highly distorted at the load that can be harmful for sensitive loads, or in severe cases, it can cause voltage collapse. Thus, performing precise load balance (including harmonics) is of great importance in making MGs reliable [11], [12]. In the grid-connected mode, the load harmonics are supplied by the grid, leading to a high quality voltage waveform at the load. However, in the islanded mode, MGs must precisely detect the amount of load harmonics and accordingly supply appropriate current (including harmonics) in order to have robust operation. It should be noted that even in the grid-connected mode, the high penetration level of intermittent RESs may pose a threat to the power network in terms of the power-quality and stability issues. Therefore, in some cases, the grid-connected RESs are required to compensate for harmonics to comply with the regulatory frameworks of the power network [13]–[16].

In order to address this issue, various harmonic compensation methods have been proposed in the literature [17]–[37]. These methods can be categorized into passive techniques [17], [18] and active techniques [19]–[37]. Active methods are more attractive as they are implemented through the control system of power electronic converters without imposing additional hardware cost to the system. The existing active methods can be categorized into the following three groups: selective harmonics compensation (SHC) [19]–[22], virtual impedance-based controllers [23]–[30], and multi-loop controllers [31]–[37].

Typically, SHC methods have been used for high power current-source converters, where the switching frequency is limited to a few hundred hertz [19]. Due to the intensive computational efforts associated with these methods, they can only compensate a few selected harmonics (e.g., fifth or seventh) [20]–[22]. Thus, they are not appropriate for MG applications where the controller should compensate for a wide range of harmonics. Harmonic compensation methods based on virtual impedance estimation have also been proposed for MGs [23]–[30]. In this approach, the converter simulates an inductive or resistive active power filter in order to produce/absorb harmonic currents [23]–[25], [27], [30]. These methods are not able to accurately inject/absorb the current harmonics and in turn create a phase shift in the compensated load voltage [28]–[30]. In addition, these methods require the load information and the grid impedance to accurately estimate virtual impedance values,

Manuscript received December 3, 2018; revised March 18, 2019 and May 7, 2019; accepted June 3, 2019. Date of publication June 18, 2019; date of current version November 12, 2019. Recommended for publication by Associate Editor L. Peng. *(Corresponding author: Sajjad Makhdoomi Kaviri.)*

S. M. Kaviri, P. K. Jain, and A. Bakhshai are with the Department of Electrical and Computer Engineering, Queen's University, Kingston ON K7L3N6, Canada (e-mail: s.makhdoomi.kaviri@queensu.ca; praveen.jain@queensu.ca; alireza.bakhshai@queensu.ca).

M. Pahlevani is with the Department of Electrical and Computer Engineering, University of Calgary, Calgary, AB T2N 1N4, Canada (e-mail: majid.pahlevani@ucalgary.ca).

Color versions of one or more of the figures in this paper are available online at http://ieeexplore.ieee.org.

Digital Object Identifier 10.1109/TPEL.2019.2923723

which in most cases are not available for the control system [25], [27], [28].

In the multi-loop control schemes, multiple control loops have been used to simultaneously regulate the fundamental component and compensate for the harmonics [31]–[37]. In order to implement these methods, the harmonic components of the load should initially be estimated [31]–[36]. In [31]–[33], the proposed multi-loop harmonic compensation approaches rely on the remote measurement of the load current. Thus, they are not very practical for MG applications. In order to solve this problem, other techniques based on the measurement of the local voltage have been introduced in [34]–[37]. However, the methods presented in [34]–[36] are only applicable to the grid-connected mode of operation as the converters have to operate in the current-controlled mode (in the islanded mode, the converters operate in the voltage-controlled mode). In [34] and [36], harmonic compensation techniques, which are based on the discrete Fourier transform (DFT) have been introduced. Although the proposed methods perform well with ideal periodic voltages, they cannot compensate for inter-harmonics and asynchronous harmonics (created by nonlinear loads). In [37], a hierarchical-based harmonic compensation method is introduced for converters operating in the voltage-controlled mode. Although this can be applicable for islanded MGs, it relies on the communication links to implement multiple control loops.

Considering the aforementioned discussions, one the main setbacks of the existing harmonic compensation methods is their inability to estimate various harmonics. Due to its importance for MG applications, precise harmonic estimations have been a very active research area. In this paper, a brief literature review for the existing harmonic estimation techniques is presented. The state-of-the-art techniques are divided into two general categories: direct approaches and indirect approaches (in which the equivalent load harmonic impedances are estimated instead of harmonics). The aforementioned methods are briefly described as follows.

A. Direct Methods

A wide range of harmonics estimation techniques have been presented in the literature. The proposed techniques utilize basic estimation techniques such as DFT [34], [38]–[40] as well as more sophisticated ones such as the Proney algorithm [41], [42], neural network (NN) [43], [44], and Kalman filter [45], [46]. Despite the simple structure of DFT-based methods, their accuracy is highly degraded for asynchronous harmonics and inter-harmonics. In order to overcome this problem, more sophisticated methods such as Proney algorithm, NN algorithm, and Kalman filtering have been proposed. However, the Proney algorithm suffers from high complexity and intensive computational efforts, the NN algorithm requires the exact model of each harmonic, and the Kalman filter based uses a complex iterative algorithm to estimate harmonics and its stability may not be guaranteed.

B. Indirect Methods

In the indirect methods, typically intentional disturbance signals are actively injected to the output to estimate the load impedances [47]–[60]. These methods use various estimation schemes such as DFT [49]–[53], window recursive DFT [54], Kalman filter [55], [56], and recursive least square [57], [58] to estimate the impedance values. The indirect methods usually require special hardware devices in order to inject disturbance signals [47], [48], [50], [58]. In addition, the precise knowledge of the background disturbances is essential for accurate results [49], [51], [59], [60]. Although the indirect methods can provide an accurate estimation of the harmonic impedances over a wide frequency range, they pollute the grid by constantly injecting harmonics, they are usually computation intensive, and they do not have fast dynamics compared to the direct techniques.

Considering the aforementioned difficulties with the existing compensation techniques, there is a need for a real-time harmonic compensation method for in islanded MGs. The compensation method should be able to estimate and compensate for various disturbances by using local measurable signals. In this paper, a novel harmonic compensation system is presented. The proposed method is able to compensate for both synchronous and asynchronous harmonics (nonlinear loads can create significant amount of asynchronous harmonics). The main contribution of the proposed harmonic compensation system is a fast hybrid load observer embedded to the proposed control system, which is able to precisely estimate the linear portion of the load and its harmonic contents in a real-time manner. The proposed control system offers a universal solution for future MGs operating in the islanded mode. The main contributions of this paper are summarized as follows.

1) A harmonic compensation system, which is able to compensate for unknown harmonics/disturbances caused by linear/nonlinear loads (e.g., synchronous and asynchronous, dc component, etc.).
2) A novel hybrid load observer that can precisely estimate the load resistance and inductance in a real-time manner.
3) The proposed observer does not pollute the grid and is autonomous (i.e., it does not rely on the communication link).
4) The proposed compensator is very practical due to its simple structure and it is not computationally intensive compared to the existing techniques.

This paper is organized as follows. The proposed harmonic compensation control method is presented in Section II. Section III describes the structure of the proposed hybrid load observer. In Section IV, the stability of the proposed compensation method has been investigated. The performance of the control system and hybrid observer are evaluated through computer simulations in Section V. The experimental results obtained from an dc/ac converter prototype are presented in Section VI. Finally, Section VII is the conclusion.

II. Proposed Harmonic Compensation System

The control of MGs in the islanded mode is challenging due to the presence of nonlinear loads and load harmonics. The control system must perform the power balance by supplying harmonics required by the loads. Otherwise, the load voltage will be highly distorted. This is not the case in the grid-connected mode where

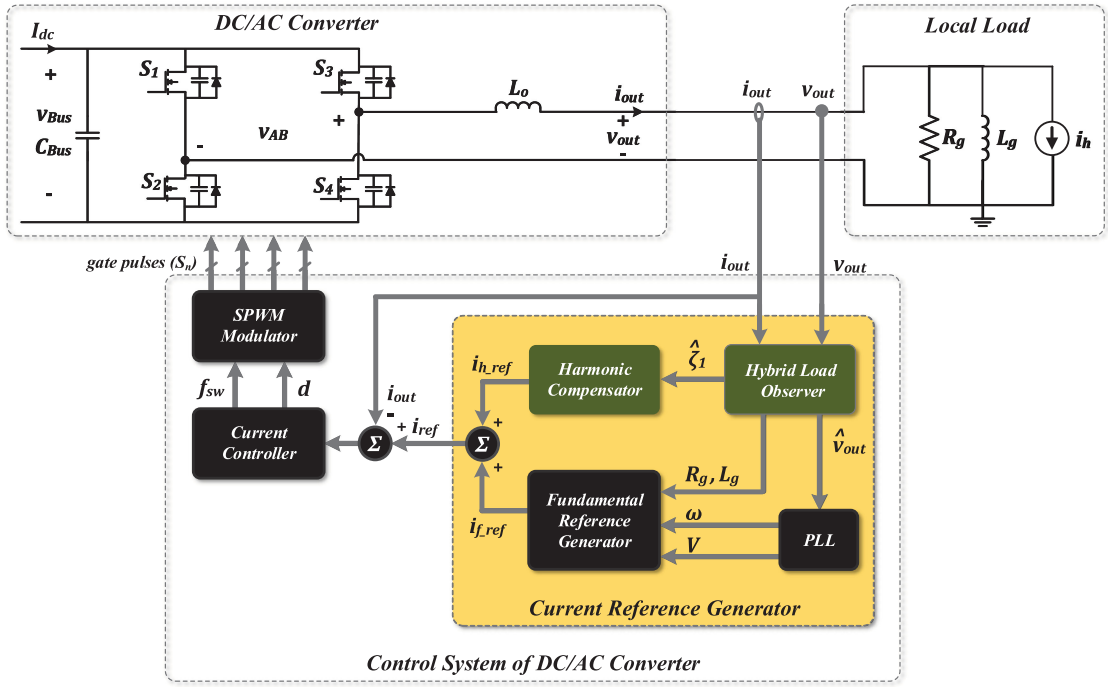

Fig. 1. Proposed harmonic compensation control scheme.

the harmonics are supplied by the grid. In this paper, a harmonic compensation system is proposed to address the aforementioned challenges. Fig. 1 shows the high-level block diagram of the proposed harmonic compensation system. According to this figure, the control system consists of a current reference generator. The current reference generator produces the reference signal, which includes the fundamental component (i.e., $i_{f-\mathrm{ref}}$) as well as the harmonic components (i.e., $i_{h-\mathrm{ref}}$) of the current. The reference signal for the harmonic components is generated using a hybrid load observer and a harmonic compensator.

The main contribution of this paper is the hybrid load observer, which estimates the harmonic contents of the load using the converter output voltage, v_{out}. The proposed observer is able to estimate unknown harmonics including synchronous and asynchronous ones. Thus, it is able to estimate special harmonics (e.g., third, fifth, etc.) as well. However, it can only estimate the full harmonic contents altogether, not a specific one. In addition, the proposed load observer estimates the linear part of the load (i.e., the load resistance, R_g, and the load inductance L_g) using the output voltage and current. Thus, the outputs of this block is the voltage harmonics contents ($\hat{\xi}_1$) as well as the output equivalent impedance (i.e., R_g and L_g). Since the load observer estimates the harmonic contents of the voltage, it can output the fundamental component (i.e., $\hat{v}_{\mathrm{out}}$) to the PLL in order to isolate the voltage harmonics from the PLL. This leads to more reliable operation of the inverter. The proposed harmonic compensation system is effective only during the islanded mode and during the transitions from the grid connected to islanded mode and vice versa, different procedures (e.g., soft-start, zero-crossing detection, etc.) have to be in place for the reliable operation.

It should be noted that although the proposed control system is derived for the single-phase inverters with L filters, it can be easily extended to the inverters with LCL filters as well as the three-phase inverters. However, in order to extend the proposed method to three-phase systems, the control system has to be either in the abc or $\alpha\beta$ reference frames. In order to implement the proposed method in three-phase systems, the same control structure proposed for single-phase systems, including the load observer, and the harmonic compensator, have to be added to the control system of each phase. The converter output voltage and current of each phase (i.e., $v_{\mathrm{out}-i}$, and $i_{\mathrm{out}-i}$, $i = a, b, c$) have to be used as input of the load observer block. In addition, the harmonic components of the current reference (i.e., $i_{h-\mathrm{ref}-i}$, $i = a, b, c$), generated by the harmonic compensator block, should be added to the fundamental current reference to form the current references for each phase.

In the following sections, the control blocks presented in Fig. 1, including the harmonic load observer, the harmonic compensator, the fundamental reference generator, and the current controller will be described in detail.

III. Proposed Hybrid Load Observer

In order to mitigate the detrimental impacts of harmonics in the islanded mode, a novel control scheme is presented in Section II. The key block in the proposed control system is the hybrid load observer, which is described in this section. The hybrid load observer is responsible for precisely estimating the linear component as well as harmonic contents of the load. The main idea is to have an unknown term representing the harmonic contents, since their nature is not known to

the control system (nonlinear loads can create various harmonics/disturbances). Thus, the output voltage is considered as a fundamental component superimposed by unknown terms representing harmonics/disturbance

$$v(t) = V\sin(\omega t + \varphi) + h(t) \tag{1}$$

where V is the voltage amplitude, ω is the line frequency, and $h(t)$ represents the harmonic contents of the measured voltage (that can include different forms of harmonics/disturbances).

In order to estimate the linear portion of the load (i.e., L_g and R_g), the linear component of the load current is given by

$$i_{\text{Lin}}(t) = i_R(t) + i_L(t) \tag{2}$$

where $i_R(t)$ represents the active component and $i_L(t)$ represents the reactive component.

Accrediting to (1) and (2), the system dynamics is derived as follows:

$$\dot{v}(t) = \omega V\cos(\omega t + \varphi) + \dot{h}(t) \tag{3}$$

$$\begin{aligned}\ddot{v}(t) &= -\omega^2 V\sin(\omega t + \varphi) + \ddot{h}(t)\\ &= -\omega^2 v(t) + \omega^2 h(t) + \ddot{h}(t)\end{aligned} \tag{4}$$

$$\begin{aligned}\dot{i}_{\text{Lin}}(t) &= \dot{i_R}(t) + \dot{i_L}(t) = \frac{1}{R_g}\dot{v}(t) + \frac{1}{L_g}v(t)\\ &= \theta_1\dot{v}(t) + \theta_2 v(t)\end{aligned} \tag{5}$$

where θ_1 and θ_2 represent the resistive component (i.e., $1/R_g$) and inductive component (i.e., $1/L_g$) of the MG linear load. The locally measurable signals are $v(t)$, $\dot{v}(t)$, and $i_{\text{Lin}}(t)$ (the digital differentiator presented in [61] has been used to generate the $\dot{v}(t)$ from the $v(t)$ signal). By using (3)–(5), the system state variables are defined as follows:

$$X^{\text{State-Variables}}: \begin{cases} x_1 = v(t)\\ x_2 = \dfrac{1}{\omega}\dot{x_1}\\ x_3 = i_{\text{Lin}}(t)\\ \xi_1 = h(t)\\ \xi_2 = \dot{\xi}_1\\ \xi_3 = \dot{\xi}_2. \end{cases} \tag{6}$$

According to (3)–(6), the system dynamics is given by

$$X^{\text{Dynamics}}: \begin{cases} \dot{x}_1 = \omega x_2\\ \dot{x}_2 = -\omega x_1 + \omega\xi_1 + \dfrac{1}{\omega}\xi_3\\ \dot{x}_3 = \theta_1 x_2 + \theta_2 x_1\\ \dot{\xi}_1 = \xi_2\\ \dot{\xi}_2 = \xi_3\\ \dot{\xi}_3 = \dddot{h}. \end{cases} \tag{7}$$

The objective is to estimate the x_1, x_2, x_3, ξ_1, θ_1, and θ_2 from the dynamics given by (7). Therefore, according to (7), the proposed load observer is given by

$$X^{\text{Dynamics}}: \begin{cases} \dot{\hat{x}}_1 = \omega\hat{x}_2 + \mu_{11}\tilde{x}_1 + \mu_{12}\tilde{x}_2\\ \dot{\hat{x}}_2 = -\omega x_1 + \omega\hat{\xi}_1 + \dfrac{1}{\omega}\hat{\xi}_3 + \mu_{21}\tilde{x}_1 + \mu_{22}\tilde{x}_2\\ \dot{\hat{x}}_3 = \hat{\theta}_1 x_2 + \hat{\theta}_2 x_1 + \mu_{31}\tilde{x}_1 + \mu_{33}\tilde{x}_3\\ \dot{\hat{\xi}}_1 = \gamma_1\omega\tilde{x}_2\\ \dot{\hat{\xi}}_2 = \hat{\xi}_3\\ \dot{\hat{\xi}}_3 = \gamma_2\dfrac{1}{\omega}\tilde{x}_2\\ \dot{\hat{\theta}}_1 = \gamma_3 x_2\tilde{x}_3\\ \dot{\hat{\theta}}_2 = \gamma_4 x_1\tilde{x}_3 \end{cases} \tag{8}$$

where $\hat{x}_i, i = 1, 2, 3$ are the estimated state variables and $\tilde{x}_i$ are estimation errors. $\hat{\xi}_1$ is the estimated harmonic contents of the grid voltage (i.e., x_1). $\hat{\theta}_1$ and $\hat{\theta}_2$ are the estimated load resistance and inductance values and $\tilde{\theta}_1$, $\tilde{\theta}_2$ are their estimation errors. According to (8), the compensating terms (i.e., $\mu_{11}\hat{x}_1$, $\mu_{12}\hat{x}_2$, $\mu_{21}\hat{x}_1$, $\mu_{22}\hat{x}_2$, $\mu_{31}\hat{x}_1$, and $\mu_{33}\hat{x}_3$) have been used in order to render the errors (i.e., $\tilde{x}_1$, $\tilde{x}_2$, and $\tilde{x}_3$) zero. The adaptive laws have also been used to estimate the values of $\hat{\xi}_1$, $\hat{\theta}_1$, and $\hat{\theta}_2$. The adaptive laws are derived to render the derivative of the Lyapunov function negative. The procedure to derive this adaptive laws will be explain in Section V in detail. μ_{11}, μ_{12}, μ_{21}, μ_{22}, μ_{31}, μ_{33}, γ_1, γ_2, γ_3, and γ_4 are compensation gains, which render the estimation errors zero. These parameters are some constant value that does not have to be exact. The proposed observer can reliably operate with different values of parameters as far as they are in the stability range. The stability range as well as the procedure to determine these gains are elaborated in Section V.

Fig. 2 shows the block diagram of the proposed load observer. According to Fig. 2, the measurable state variables $x_1(t) = v(t)$, $x_2(t) = \dot{v}(t)$, and $x_3(t) = i_{\text{Lin}}(t)$ are the inputs to the observer block. The outputs are the estimated variables $\hat{x}_1, \hat{x}_3, \hat{\xi}_1, \hat{\theta}_1$, and $\hat{\theta}_2$.

It should be noted that the performance of the proposed observer is not dependent on the precise values of ω since the compensation terms will compensate any discrepancy in the frequency value up to some limits (ω is considered as a predefined constant value in the observer block). This is a very advantageous for MGs where the frequency can have a wide range of variations.

IV. Proposed Control System

In this paper, a control system including a harmonic compensation system is proposed for single-phase inverters operating in the islanded mode. According to Fig. 1, the proposed control system includes the harmonic compensator and the fundamental reference generator that generate the current reference, as well as the current controller that regulates the converter output current. In the following subsections, the aforementioned control blocks are explained in detail.

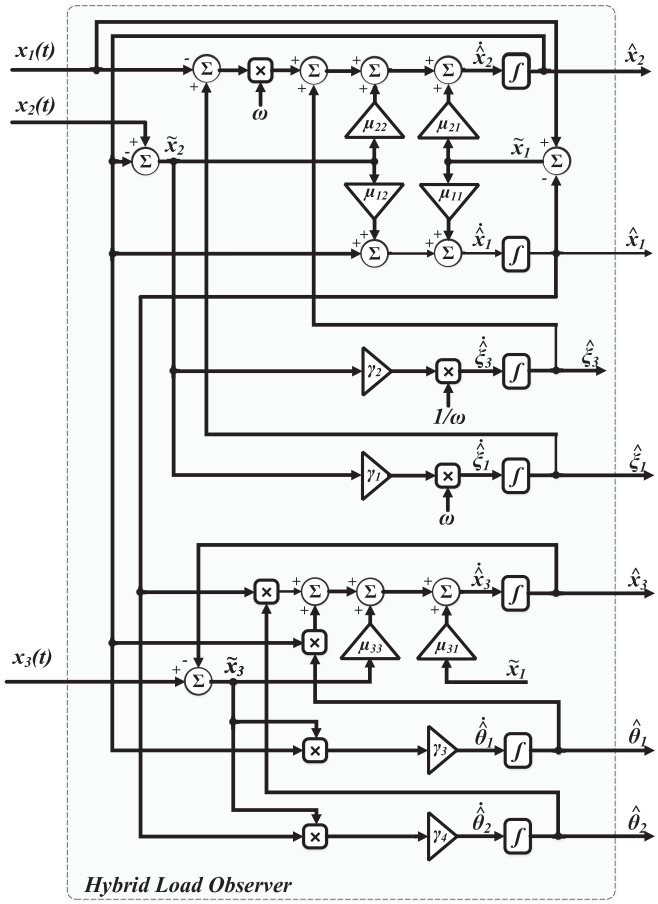

Fig. 2. Block diagram of the proposed hybrid load observer.

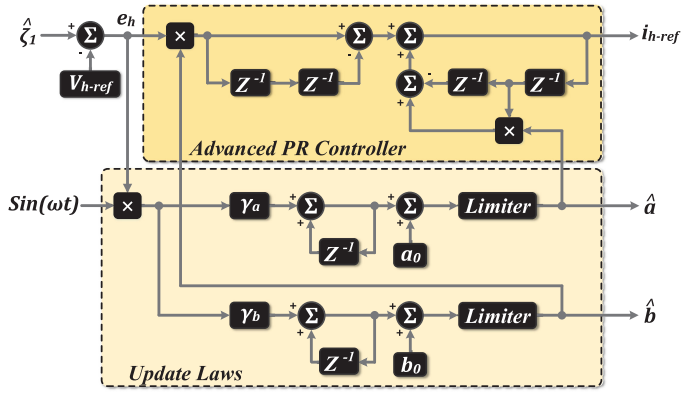

Fig. 3. Digital implementation of the adaptive PR controller utilized as a harmonic compensator [67].

A. Harmonic Compensator

The harmonic compensator is responsible for generating the harmonic components of the current reference signal (i.e., $i_{h-\mathrm{ref}}$) using the harmonic contents of the converter output signal (i.e., $\hat{\xi}_1$). Thus, the input of this block is the voltage harmonic content produced by the hybrid load observer block. Conventionally, several proportional-resonant (PR) controllers tuned at harmonic frequencies, have widely been used as the harmonic compensator [34], [62]–[64]. Due to the structure of the PR controller, where the relation between the input signal and the generated output signal can be nonlinear, these controllers are the appropriate options for using as harmonic compensators. The conventional control structure can offer the nearly perfect tracking of the reference signal by using one PR controller for each harmonic frequency. However, due to the difficulties with digital implementation of the PR controllers (e.g., extensive utilization of resources), and stability concerns (e.g., when the harmonic frequency is out of the bandwidth of the controller), the application of this structure is limited to the several low-order synchronized harmonics (e.g., third, fifth, and seventh) [65]–[67]. This structure also needs separate reference signals for each harmonic, which is not available through the proposed hybrid observer. In addition, the adverse impact of the grid frequency variations on the tracking performance of PR controllers, is another limitation of this control system in islanded MGs, where the line frequency can change in a considerable range [67].

In order to mitigate the drawbacks of the conventional harmonic compensation system, the adaptive PR controller proposed in [67] has been used in this paper. This controller is fully compatible with the proposed structure as it can track synchronous and asynchronous harmonics without the need to individual harmonic references. In the implemented controller, the perfect tracking for the harmonic components of the input signal is achieved by providing high gains for different harmonic components (e.g., synchronous and asynchronous). Fig. 3 shows the block diagram of the digital implementation of the controller presented in [67].

According to Fig. 3, in order to address the drawbacks with the conventional PR-based compensators, the presented controller is based on the adaptive variation of PR coefficients according to the reference signal tracking error. The continuous updating of the PR coefficients enables this controller to provide the high flexibility needed to compensate for a wide range of synchronous and asynchronous harmonics. It also enables the compensator to remove the tracking error produced by changes in the grid frequency and provide compensation for any dc component of the reference signal (typically proportional-integral (PI) controllers are added to compensate for dc components). Therefore, the presented compensator offers a simple structure, as well as a superior tracking performance over a fairly wide range of harmonics that eliminates the need for using multiple PR controllers.

According to Fig. 3, the update laws have been used to generate the coefficients of the harmonic compensator. The update laws utilize the value of the reference signal error to make adjustments to the nominal coefficients such that the steady-state error is rendered zero. The update laws are given by

$$\dot{\hat{a}} = \gamma_a e_h \sin(\omega t) \tag{9}$$

$$\dot{\hat{b}} = \gamma_b e_h \sin(\omega t) \tag{10}$$

where $\dot{\hat{a}}$ and $\dot{\hat{b}}$ are the adaptive coefficients of the PR controller, γ_a and γ_b are the controller constant gains, and e_h is the reference signal tracking error. According to Fig. 3, the γ_a and in

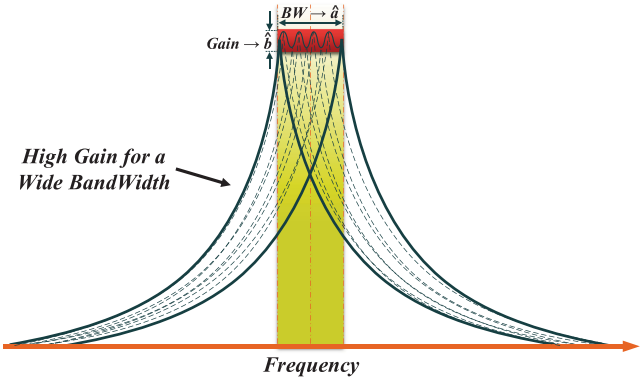

Fig. 4. Virtual bode plot resulting from the proposed adaptive PR controller [67].

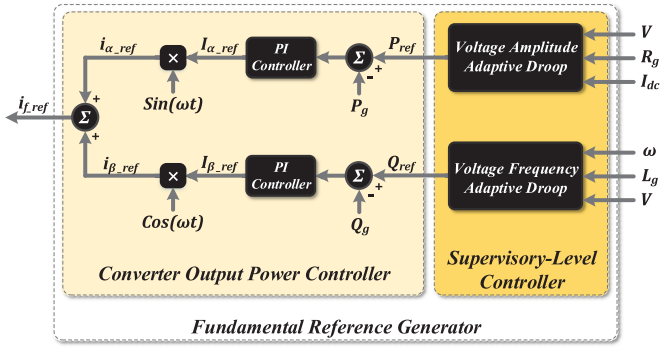

Fig. 5. Fundamental reference generator control scheme.

turn $\dot{\hat{a}}$ determines the speed of the convergence in the center frequency, while γ_a and in turn $\dot{\hat{b}}$ determines the steady-state tracking error. Therefore, for the particular design in this paper, these values are selected as $\gamma_a = 0.45$, and $\gamma_b = 1.65$ in order to compensate high-order harmonics (i.e., 39th harmonic component) with negligible tracking error. The initial points of a_0 and b_0 are also selected as $a_0 = -1.99$ and $b_0 = 1.24e-5$ as defined in [67] for the 60–Hz power conditioning systems. The procedure to select the controller coefficients are described in [67] in detail.

It should be noted that, due to the limitations of the digital implementation of the proposed compensator and the current controller (e.g., truncation of coefficients, limited number of bits, and the current controller limited bandwidth), the excellent compensation performance can only be achieved in a limited range of harmonics. In order to avoid generating the current reference terms out of the current controller bandwidth, a low-pass filter tuned at the cutoff frequency of the current controller has been added to the compensation system. Considering the required filtering in designing the compensation system, the high performance can be maintained for the aforementioned harmonics.

According to the specified coefficients, the presented adaptive droop structure eliminates the need for having very precise coefficients for each harmonic frequency, which highly reduce the number of resources required for the digital implementation of the harmonic compensator using the adaptive PR controller. According to (9) and (10), the bandwidth of the PR controller is increased virtually to achieve a very high gain at the desired harmonic frequency. Fig. 4 shows the virtual bode plot resulting from changing the coefficients of the compensator (e.g., $\dot{\hat{a}}$ and $\dot{\hat{b}}$) adaptively. According to this figure, the bandwidth and the gain of the adaptive PR controller can be effectively controlled for a wide range of harmonic frequencies [67].

It should be noted that due to the structure of the proposed hybrid observer and the compensation system, a simple PI controller can also be used as the harmonic compensator. However, due to the limitations of the digital implementation of PI controllers (especially in higher order harmonics), in case of using the PI compensator, the application of the compensation system will be limited to several low-order harmonics (e.g., third, fifth, and seventh).

B. Fundamental Reference Generator

The fundamental reference generator is responsible for regulating the amplitude and frequency of the MG voltage by producing an appropriate reference signal for the current controller (i.e., $i_{f-\mathrm{ref}}$). Fig. 5 shows the block diagram of the implemented control system for the fundamental reference generator block. According to this figure, the implemented control structure includes two controllers, the converter output power controller, and the supervisory-level controller. The converter output power controller regulates the flow of the power between the converter and the MG by providing the sinusoidal current reference to the current controller (i.e., $i_{f-\mathrm{ref}}$). The supervisory-level controller deals with MG parameters regulation (e.g., amplitude and frequency of the MG voltage [i.e., V and ω)]. The implemented supervisory-level controller uses the voltage amplitude/frequency adaptive droop controllers to regulate the MG voltage amplitude and frequency.

According to Fig. 5, the supervisory-level controller performs its control tasks by providing the required set points of the power controller (i.e., the output active/reactive power references, P_{ref} and Q_{ref}). The detailed control structure of the fundamental current reference generator block including the supervisory-level controller and the power controller is described in [68] and [69] in detail.

C. Current Controller

The current controller is responsible for regulating the converter output current based on the current reference signal, which includes the fundamental component ($i_{f-\mathrm{ref}}$) provided by the fundamental reference generator, and the harmonic components ($i_{h-\mathrm{ref}}$) provided by the harmonic compensator. Due to the structure of the proposed control system (illustrated in Fig. 1), the same control structure adopted for harmonic compensator can be implemented for the current controller to achieve a perfect tracking of the reference signal over a wide range of harmonic components. The same coefficient defined for the harmonic compensator can also be used for the current controller.

It should be noted that a conventional PR controller can also be used for the current controller. By selecting the relatively high gains for PR controller, it will be capable of tracking the low-order harmonic components of the reference signal, but due to the limitation of the digital implementation of PR controllers, this control structure is only applicable for compensating several low-order harmonics (e.g., third, fifth, and seventh).

V. Stability Analysis of the Proposed Hybrid Load Observer

The stability of the proposed observer is analyzed in this section. Since the hybrid load observer is a nonlinear system, the Lyapunov stability approach is used to analyze the system stability [70], [71]. According to (7) and (8), the error dynamics is given by

$$\tilde{X}^{\text{Error}}: \begin{cases} \dot{\tilde{x}}_1 = \omega\tilde{x}_2 - \mu_{11}\tilde{x}_1 - \mu_{12}\tilde{x}_2 \\ \dot{\tilde{x}}_2 = \omega\tilde{\xi}_1 + \dfrac{1}{\omega}\tilde{\xi}_3 - \mu_{21}\tilde{x}_1 - \mu_{22}\tilde{x}_2 \\ \dot{\tilde{x}}_3 = \tilde{\theta}_1 x_2 + \tilde{\theta}_2 x_1 - \mu_{31}\tilde{x}_1 - \mu_{33}\tilde{x}_3 \\ \dot{\tilde{\xi}}_1 = -\gamma_1\omega\tilde{x}_2 \\ \dot{\tilde{\xi}}_3 = -\gamma_2\dfrac{1}{\omega}\tilde{x}_2 \\ \dot{\tilde{\theta}}_1 = -\gamma_3 x_2\tilde{x}_3 \\ \dot{\tilde{\theta}}_2 = -\gamma_4 x_1\tilde{x}_3. \end{cases} \tag{11}$$

The Lyapunov candidate (energy function) is defined based on the errors

$$V = \frac{1}{2}\tilde{x}_1^2 + \frac{1}{2}\tilde{x}_2^2 + \frac{1}{2}\tilde{x}_3^2 + \frac{1}{2\gamma_1}\tilde{\xi}_1^2 + \frac{1}{2\gamma_2}\tilde{\xi}_3^2 + \frac{1}{2\gamma_3}\tilde{\theta}_1^2 + \frac{1}{2\gamma_4}\tilde{\theta}_2^2. \tag{12}$$

The derivative of the Lyapunov function is derived as

$$\dot{V} = \tilde{x}_1\dot{\tilde{x}}_1 + \tilde{x}_2\dot{\tilde{x}}_2 + \tilde{x}_3\dot{\tilde{x}}_3 + \frac{1}{\gamma_1}\tilde{\xi}_1\dot{\tilde{\xi}}_1 + \frac{1}{\gamma_2}\tilde{\xi}_3\dot{\tilde{\xi}}_3 + \frac{1}{\gamma_3}\tilde{\theta}_1\dot{\tilde{\theta}}_1 + \frac{1}{\gamma_4}\tilde{\theta}_2\dot{\tilde{\theta}}_2. \tag{13}$$

By inserting the error dynamics of $\dot{\tilde{x}}_1$, $\dot{\tilde{x}}_2$, and $\dot{\tilde{x}}_3$, given by (11), in (13), the derivative of the Lyapunov function is derived as

$$\begin{aligned} \dot{V} = {} & \left((-\mu_{11})\tilde{x}_1^2 + (-\mu_{22})\tilde{x}_2^2 + (-\mu_{33})\tilde{x}_3^2\right) \\ & + \left((\omega - \mu_{12} - \mu_{21})\tilde{x}_1\tilde{x}_2 + (-\mu_{31})\tilde{x}_1\tilde{x}_3\right) \\ & + \left(\left(\omega\tilde{x}_2 + \frac{1}{\gamma_1}\dot{\tilde{\xi}}_1\right)\tilde{\xi}_1\right) + \left(\left(\frac{1}{\omega}\tilde{x}_2 + \frac{1}{\gamma_2}\dot{\tilde{\xi}}_3\right)\tilde{\xi}_3\right) \\ & + \left((x_2\tilde{x}_3 + \frac{1}{\gamma_3}\dot{\tilde{\theta}}_1)\tilde{\theta}_1\right) + \left((x_1\tilde{x}_3 + \frac{1}{\gamma_4}\dot{\tilde{\theta}}_2)\tilde{\theta}_2\right). \end{aligned} \tag{14}$$

In order to make the derivative of the Lyapunov function ($\dot{V}$) negative semi-definite, appropriate functions should be selected for $\dot{\tilde{\xi}}_1$, $\dot{\tilde{\xi}}_3$, $\dot{\tilde{\theta}}_1$, and $\dot{\tilde{\theta}}_2$. Therefore, to make $\dot{V}$ negative semi-definite, the selected functions presented by (11) are used. Thus, the derivative of the Lyapunov function is given as

$$\begin{aligned} \dot{V} = {} & \left(\left(\frac{-\mu_{11}}{2}\right)\tilde{x}_1^2 + (\omega - \mu_{12} - \mu_{21})\tilde{x}_1\tilde{x}_2 + (-\mu_{22})\tilde{x}_2^2\right) \\ & + \left(\left(\frac{-\mu_{11}}{2}\right)\tilde{x}_1^2 + (-\mu_{31})\tilde{x}_1\tilde{x}_3 + (-\mu_{33})\tilde{x}_3^2\right). \end{aligned} \tag{15}$$

By using the selected functions for $\dot{\tilde{\xi}}_1$, $\dot{\tilde{\xi}}_3$, $\dot{\tilde{\theta}}_1$, and $\dot{\tilde{\theta}}_2$, the derivative of the Lyapunov function ($\dot{V}$) is presented in the quadratic form. Thus, the boundaries of the observer gains can be derived in a way to make the derivative negative semi-definite [70], [71]. The boundaries of the observer are given as

$$\mu_{11} \geq 0, \quad \mu_{22} \geq 0 \quad \text{and} \quad \mu_{33} \geq 0 \tag{16}$$

$$\mu_{12} - \mu_{21} \geq \omega - \sqrt{2\mu_{11}\mu_{22}} \tag{17}$$

$$\mu_{31} \geq \sqrt{2\mu_{11}\mu_{33}}. \tag{18}$$

The observer gains (i.e., μ_{11}, μ_{22}, μ_{33}, μ_{12}, μ_{21}, and μ_{31}) must be tuned within the ranges determined by (16)–(18). According to the error dynamics given in (11) and $\dot{V}$ given in (15), the speed of the convergence for the $\hat{x}_1$, $\hat{x}_2$, and $\hat{x}_3$ is related to the coefficients, (μ_{11}, μ_{12}), (μ_{21}, μ_{22}), and (μ_{31}, μ_{33}), respectively. While, the values of γ_1, γ_2, γ_3, and γ_4 determine the speed of convergence for $\hat{\zeta}_1$, $\hat{\zeta}_2$, $\hat{\theta}_1$, and $\hat{\theta}_2$, respectively. Due to the structure of the proposed observer the tuning of the observer gains is not a challenging task. Once the gains have been tuned in the specified range, the accurate performance and the convergence of the estimated parameters are guaranteed. Further adjustments on these parameters can be performed to achieve the desired convergence speed for different variables. To achieve the best results, the tuning process can be started by first tuning the (μ_{21}, μ_{22}), and then, the (μ_{11}, μ_{12}) and (μ_{31}, μ_{33}) gains. Once the desired estimated results of $\hat{x}_1$, $\hat{x}_2$, and $\hat{x}_3$ are achieved (in terms of accuracy and the speed of convergence), γ_1, γ_2, γ_3, and γ_4 can be tuned to achieve the accurate and fast estimation of $\hat{\zeta}_1$, $\hat{\zeta}_2$, $\hat{\theta}_1$, and $\hat{\theta}_2$.

Using the aforementioned constraints only guarantee the boundedness of the errors and their asymptotic stability still needs to be addressed [72]. Since, the proposed load observer structure is a time-variant system (according to (11) where θ_1 and θ_2 are the time variant parameters), the Barbalat's Lemma theorem can be used to evaluate the asymptotic stability of the system [73]. According to the Barbalat's Lemma theorem, the asymptotic stability of the error system can be guaranteed if the time-variant Lyapunov function ($V(t)$) satisfies the following conditions [73]:

1) $V(t)$ is lower bounded;
2) $\dot{V}(t)$ is negative semi-definite;
3) $\ddot{V}(t)$ is finite.

According to (12)–(15), the defined Lyapunov function is negative semi-definite and lower bounded. Therefore, to prove the asymptotic stability, $\ddot{V}(t)$ must be finite. According to (15), $\ddot{V}(t)$ is derived as

$$\begin{aligned} \ddot{V} = {} & -2\mu_{11}\tilde{x}_1\dot{\tilde{x}}_1 + (\omega - \mu_{12} - \mu_{21})(\tilde{x}_2\dot{\tilde{x}}_1 + \tilde{x}_1\dot{\tilde{x}}_2) \\ & - 2\mu_{22}\tilde{x}_2\dot{\tilde{x}}_2 - 2\mu_{33}\tilde{x}_3\dot{\tilde{x}}_3 - 2\mu_{31}(\tilde{x}_1\dot{\tilde{x}}_3 + \tilde{x}_3\dot{\tilde{x}}_1). \end{aligned} \tag{19}$$

By inserting the error dynamics from (11) into (19), $\ddot{V}(t)$ is given by

$$\begin{aligned}\ddot{V} = &\left(2\mu_{11}^2+\mu_{31}^2+\mu_{21}^2+\mu_{21}(\mu_{12}-\omega)\right)\tilde{x}_1^2\\ &+\left(\omega^2+\mu_{12}^2+2\mu_{22}^2-(1+\omega)\mu_{12}+\mu_{21}(\mu_{12}-1)\right)\tilde{x}_2^2\\ &+(-(2+\omega)\mu_{11}-\omega\mu_{22}+(3\mu_{11}+\mu_{22})\mu_{12}+\tilde{x}_1\tilde{x}_2\\ &+(3\mu_{22}+\mu_{11})\mu_{21})\,\tilde{x}_1\tilde{x}_2+(\mu_{31}\omega+\mu_{31}\mu_{12})\,\tilde{x}_2\tilde{x}_3\\ &+\left(2\mu_{33}^2\right)\tilde{x}_3+(3\mu_{31}\mu_{33}+\mu_{33}\mu_{11})\,\tilde{x}_1\tilde{x}_3\\ &+\left(\omega^2-\omega(\mu_{12}+\mu_{21})\right)\tilde{x}_1\tilde{\xi}_1+(-2\mu_{22})\,\tilde{x}_2\tilde{\xi}_1\\ &+\left(1-\frac{1}{\omega}(\mu_{12}+\mu_{21})\right)\tilde{x}_1\tilde{\xi}_3+\left(\frac{-2}{\omega}\mu_{22}\right)\tilde{x}_2\tilde{\xi}_3\\ &+(-2\mu_{33}x_2)\,\tilde{x}_3\tilde{\theta}_1+(-2\mu_{33}x_1)\,\tilde{x}_3\tilde{\theta}_2\\ &+(-\mu_{31}x_2)\,\tilde{x}_1\tilde{\theta}_1+(-\mu_{31}x_1)\,\tilde{x}_1\tilde{\theta}_2. \qquad (20)\end{aligned}$$

Since all the terms in (20) is bounded, $\ddot{V}$ is bounded. Thus, according to the Barbalat's Lemma, the errors (i.e., $\tilde{\xi}_1$ and $\tilde{\xi}_3$) are asymptotically stable.

Although the asymptotic stability of the error signals have been proven, the convergence of the parameters (i.e., $\tilde{\theta}_1$ and $\tilde{\theta}_2$) are not guaranteed. In order to address this issue, the persistency of excitation (PE) theorem is used to prove the convergence of the parameters to their actual values [72]. According to the PE theorem, the global asymptotic stability can be guaranteed if the update laws are persistently excited. In particular, based on the PE theorem the following condition must be met to guarantee the persistency of excitation for a scalar function $\phi(t)$:

$$\int_t^{t+T}\phi^2(\tau)d\tau \geq \eta > 0 \qquad (21)$$

where T and η are positive real values.

Since, all the input signals of the proposed hybrid load observer (x_1, x_2, and x_3) are trigonometric signals with the frequency of ω, the aforementioned condition for the PE theorem is satisfied. In particular, for the estimated grid impedance parameters (i.e., $\hat{\theta}_1$ and $\hat{\theta}_2$), the PE theorem condition can be met according to the presence of trigonometric signals, x_1 and x_2 in (8). For instance, in the adaptive law (8) for θ_1, the scalar function $\phi(t)$ is defined as: $\phi(t) = -\omega V\cos(\omega t+\phi)$, and the PE theorem condition is derived as follows:

$$\int_t^{t+\frac{2\pi}{\omega}}(\omega V)^2\cos^2(\omega\tau+\phi)d\tau = \frac{\pi}{\omega}(\omega V)^2 > 0. \qquad (22)$$

Using the same method, $\phi(t)$ can be defined as: $\phi(t) = -V\sin(\omega t+\phi)$ for θ_2, and the PE theorem condition is given by

$$\int_t^{t+\frac{2\pi}{\omega}}(V)^2\sin^2(\omega\tau+\phi)d\tau = \frac{\pi}{\omega}(V)^2 > 0. \qquad (23)$$

According to the PE theorem, the global asymptotic stability of the estimated parameters (i.e., $\hat{\theta}_1$ and $\hat{\theta}_2$) is guaranteed.

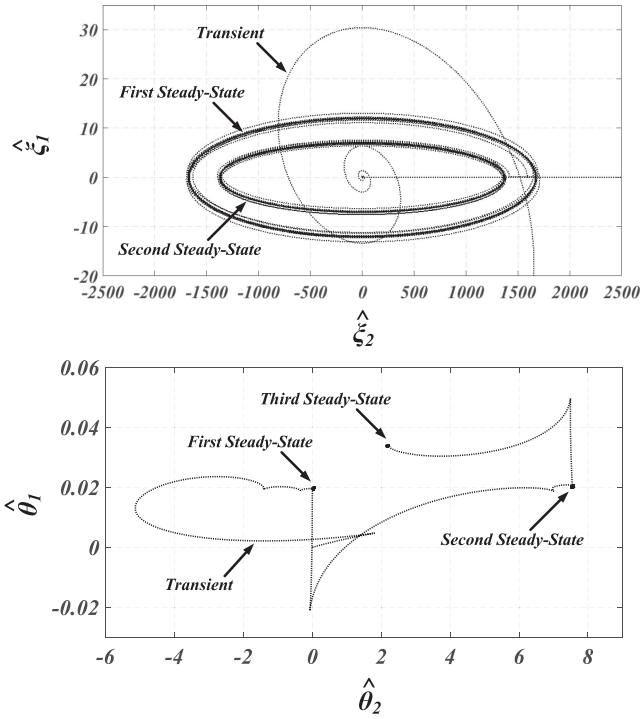

Fig. 6. Trajectory of the proposed hybrid observer.

TABLE I
PARAMETERS OF THE SIMULATED DC/AC CONVERTER

Symbols	Parameters	Values
P_o	Rated Output Power	1 kW
f_{sw}	Switching Frequency	20 kHz
v_{out}	Rated MG Voltage	240 V AC
v_{Bus}	DC-Bus Voltage	400 V DC
L_o	Output Inductor	4 mH
C_{Bus}	DC-bus Capacitor	400 μF

Fig. 6 shows the trajectory of the proposed hybrid observer. This figure illustrates how the system is steered from one steady-state condition to another one with different harmonic contents and different equivalent load values.

VI. PERFORMANCE EVALUATION THROUGH SIMULATION RESULTS

In this section, the performance of the proposed control scheme with the embedded hybrid load observer has been evaluated using PSIM and MATLAB software packages. The specifications of the dc/ac inverter in the simulations are given in Table I.

Fig. 7(a) and (b) shows the transient performance of the hybrid load observer for estimating the harmonic contents of the voltage when harmonics are present. In particular, in Fig. 7(a), a 5% fifth harmonic component has been superimposed to the voltage (x_1) and to the current (x_3) at $t = 0.08$ s, and a 4% seventh harmonic component, and a 4% ninth harmonic component have been superimposed to the voltage and to the current

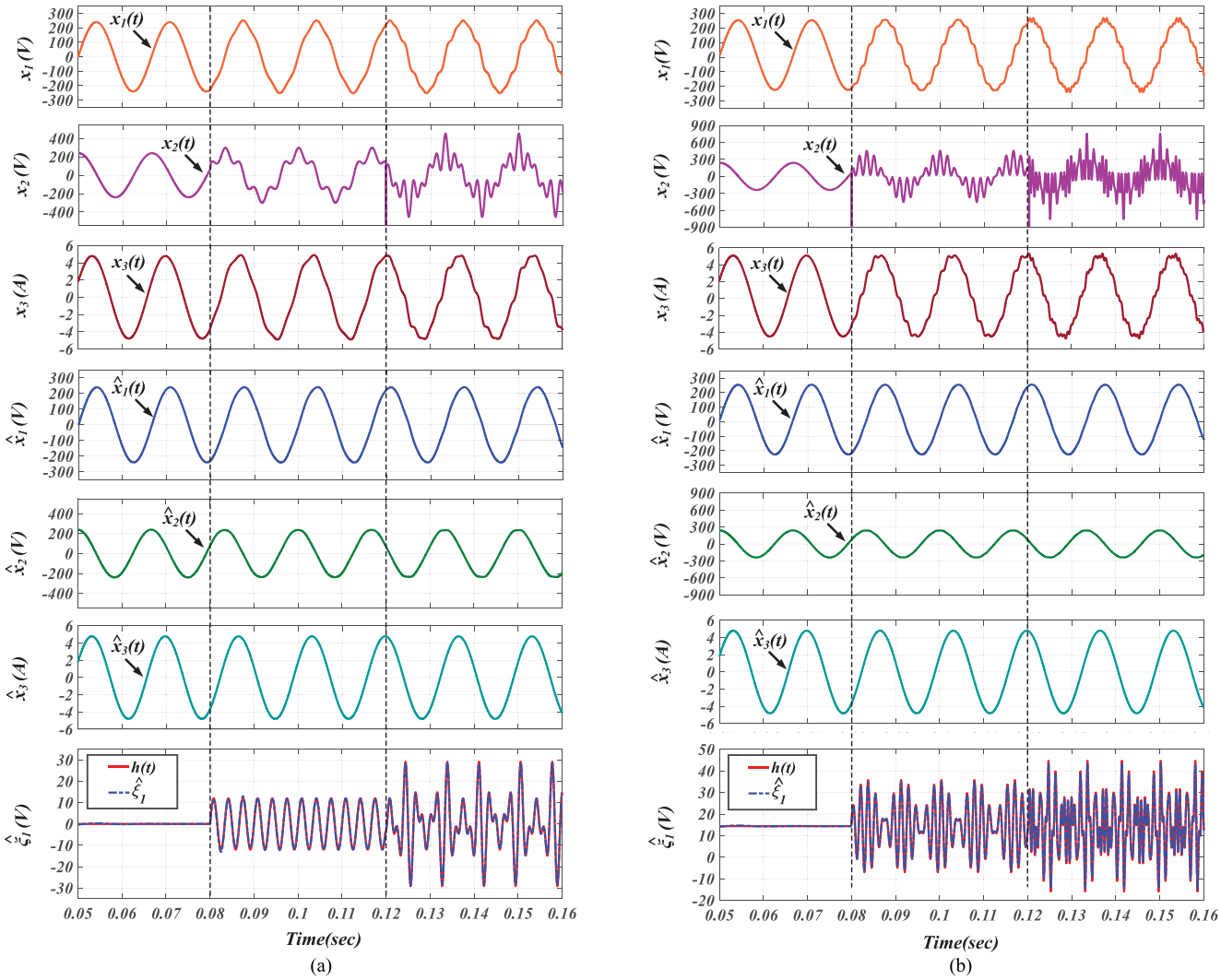

Fig. 7. Transient performance of the proposed observer when: (a) 5% fifth harmonic component is applied at $t = 0.08$ s and a 4% seventh harmonic component, and a 4% ninth harmonic component is applied at $t = 0.12$ s, and (b) 6% dc component is applied at $t = 0$ s, a 5% ninth harmonic component and a 5% eleventh harmonic component are applied at $t = 0.08$ s, and a 3% nineteenth harmonic component, a 3% twenty-third harmonic component, and a 2% asynchronous harmonic with the frequency of 1495 Hz are applied at $t = 0.12$ s.

at $t = 0.12$ s. According to Fig. 7(a), the applied harmonics are much more pronounced in the x_2 (since x_2 is the derivative of x_1). In Fig. 7(b), a 6% dc component is applied at $t = 0$ s, a 5% ninth harmonic component and a 5% eleventh harmonic component are applied at $t = 0.08$ s, and a 3% nineteenth component, a 3% twenty-third component, and a 2% asynchronous harmonic component with the frequency of 1495 Hz are applied at $t = 0.12$ s. Fig. 7(a) and (b) demonstrates the capability of the proposed observer in precisely tracking various harmonics/disturbances. Thus, the proposed hybrid observer can extract the fundamental components (i.e., $\hat{x}_1$, $\hat{x}_2$, and $\hat{x}_3$) from the polluted signals. Fig. 7 also depicts the estimated ($\hat{\xi}_1$) and actual ($h(t)$) harmonic contents. This figure shows the fast and accurate tracking of the proposed hybrid observer in on-line tracking of various load harmonics.

Fig. 8 shows the fundamental components estimation performance in two line cycles. In this figure, an extreme case for harmonics is presented (a 10% fifth harmonic component, an 8% seventh harmonic component, and an 8% ninth harmonic component have been applied to the input signals). According to this figure, despite the heavily polluted input signals, the proposed observer are able to extract the fundamental components with negligible amount of harmonic contents.

Fig. 9 shows the transient performance of the proposed hybrid observer for estimating the linear portion of the load (i.e., $\hat{\theta}_1$ and $\hat{\theta}_2$). In this figure, the resistive load value has been changed from 100 to 40 Ω at $t = 0.2$ s, and from 40 to 400 Ω at $t = 0.3$ s. In addition, the inductive load value has also varied from 100 to 250 mH at $t = 0.1$ s, and from 250 to 50 mH at $t = 0.3$ s. According to Fig. 9, the proposed hybrid observer can accurately track changes in the load impedance. Since the hybrid load observer utilizes the extracted fundamental components ($\hat{x}_1$ and $\hat{x}_3$) to estimate the load impedance, the estimations are robust against harmonic contents.

Fig. 10 evaluates the robustness of the proposed observer in the estimation of the specified parameters (e.g., harmonic

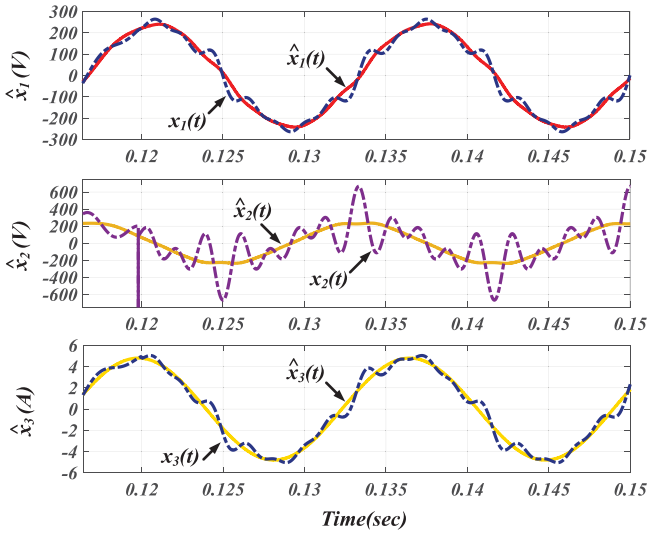

Fig. 8. Fundamental component extraction when a 10% fifth harmonic component, an 8% seventh harmonic component, and an 8% ninth harmonic component are applied to the input signals.

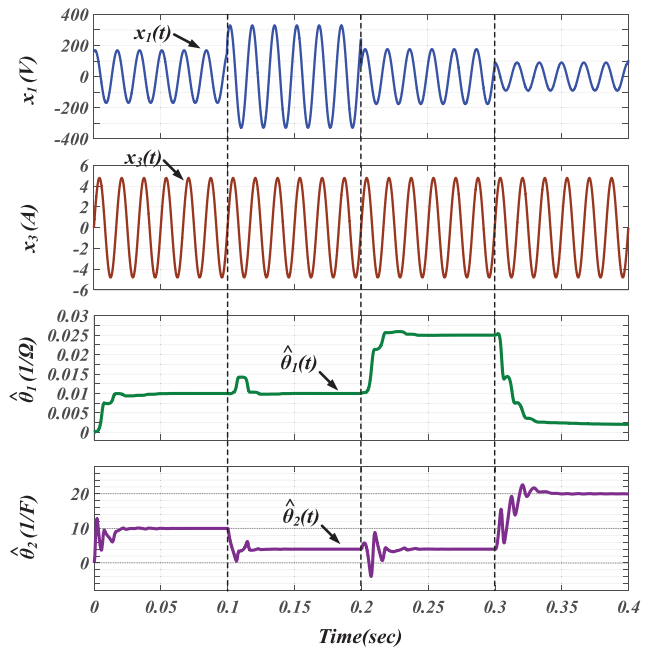

Fig. 9. Transient performance of the proposed observer for estimating the linear portion of the local load.

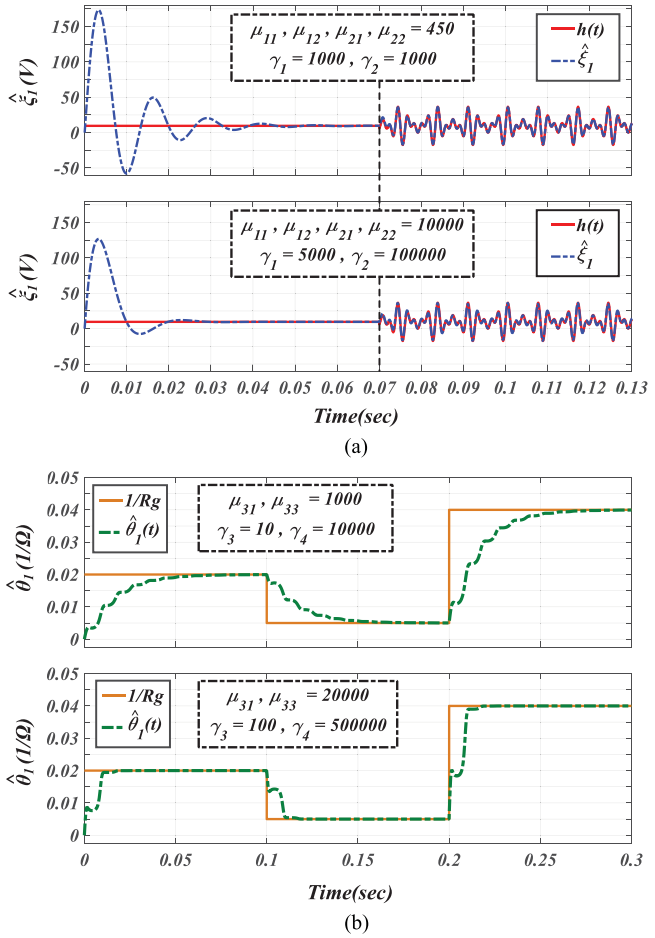

Fig. 10. Robustness of the proposed observer, against variation of the observer gains, in (a) estimation of the voltage harmonic contents when a 4% dc component is applied at $t = 0$ s and a 4% fifth harmonic component, a 4% seventh harmonic component, and a 4% ninth harmonic component are applied at $t = 0.07$ s, and (b) estimation of the linear portion of the local load ($\hat{\theta}_1$) when the resistive load value has been changed from 50 to 100 Ω at $t = 0.1$ s and from 100 to 25 Ω at $t = 0.2$ s.

contents, and linear portion of local load), against variation of the observer gains. According to this figure, the proposed observer can reliably operate with different values of observer gains as far as they are in the specified stability range. According to the waveforms presented in Fig. 10, by further adjustments on observer gains (i.e., increasing the compensation gains), the more dominant compensation terms and in turn a faster convergence speed can be achieved. It should be noted that, in practical cases, the higher observer gains will lead to the higher amplification of the input signal noises. Therefore, in these applications, the observer gains should be limited to an upper threshold to mitigate the disruptive effects of the noises.

Fig. 11(a)–(d) shows the transient performance of the harmonics compensator when two different sets of harmonic components have been applied to the load. Fig. 11(a) and (c) shows the waveforms when the harmonic compensator is disabled and Fig. 11(b) and (d) depicts the waveforms when the proposed harmonic compensator is enabled. According to this figure, the proposed harmonic compensator can effectively compensate for the harmonics and provide very reliable operation in the presence of harmonics.

Table II compares the performance of the proposed harmonic compensation system with the control system presented in [34], in terms of harmonic compensation percentage. In order to evaluate the performance of the proposed system for a wide range of load harmonics in the MG, four different cases with various harmonics orders and various percentages of harmonics is considered in Table II. According to the results presented in [34], unlike other presented methods in the literature, this method

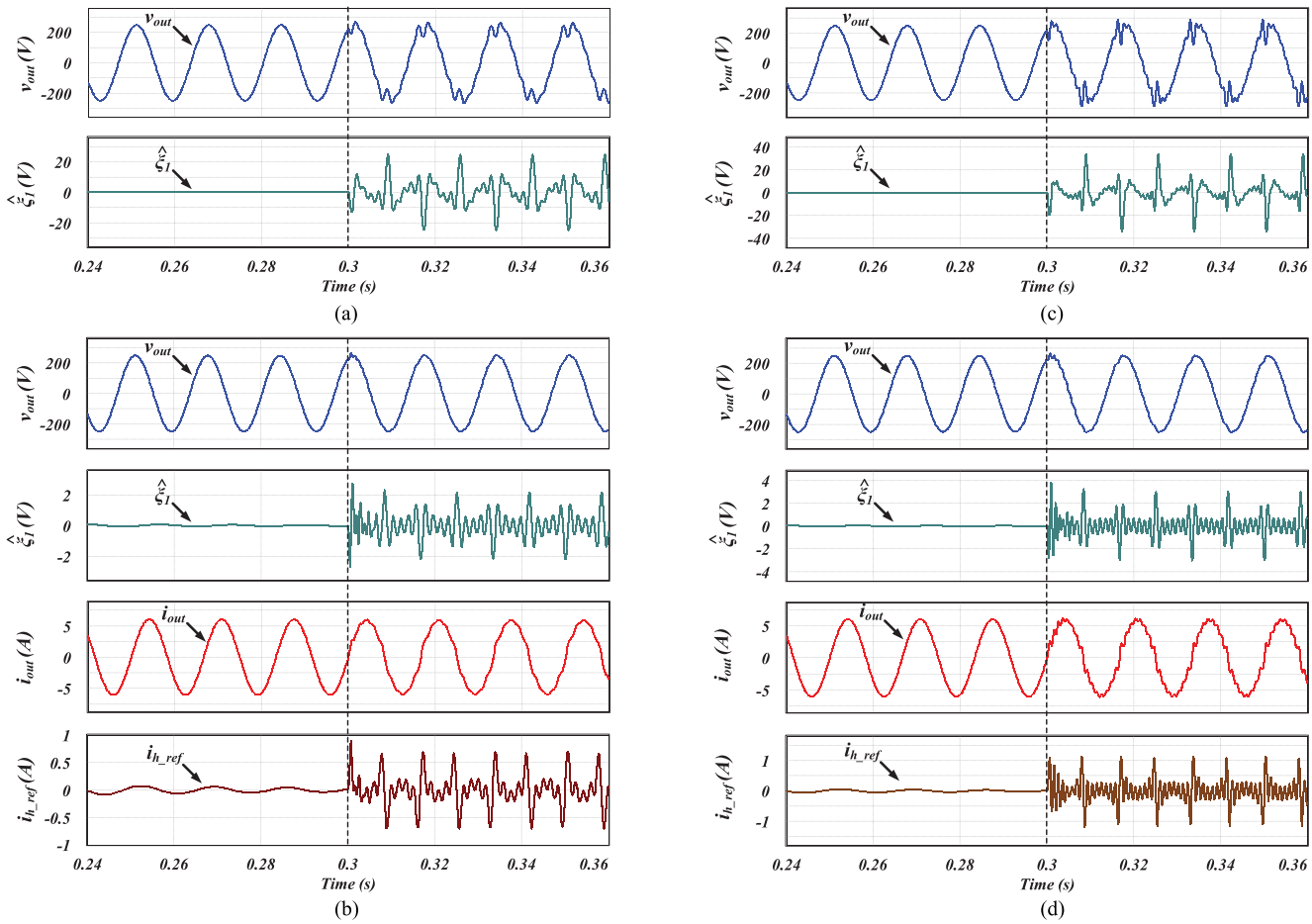

Fig. 11. Transient performance of the proposed harmonic compensation system when a 4% third harmonic component, a 3% fifth harmonic component, a 3% seventh harmonic component, and a 3% ninth harmonic component are applied at $t = 0.3$ s when compensation is (a) disabled and (b) enabled, and when a 4% third harmonic component, and a 3% fifth harmonic component, a 3% seventh harmonic component, a 3% ninth harmonic component, a 3% eleventh harmonic component, a 3% thirteenth harmonic component, and a 3% fifteenth harmonic component are applied at $t = 0.3$ s when compensation is (c) disabled and (d) enabled.

offers the compensation of harmonics in a fair range of harmonics frequencies. Thus, the results of this method are compared with the results obtained from the proposed system. According to Table II, the proposed method offers a superior performance over a wide range of synchronous and asynchronous harmonics, while the application of the method presented in [34] is limited to a couple of low-order synchronous harmonics.

VII. Experimental Results

In order to verify the feasibility of the proposed control system and evaluate its performance, it is implemented on an experimental prototype. The specifications of the implemented inverter are given in Table III. The configuration of the implemented single-phase MG is shown in Fig. 12. Since the main focus of this paper is on small-scale MG systems used in residential and commercial applications, the MG loads have been approximated as lumped loads in Fig. 12 [74]–[77]. According to this figure, the experimental results presented in this section is obtained from the indicated solar converter. Fig. 13 shows the experimental prototype of the inverter and the MG setup (i.e., the inverters and MG dynamic loads). According to this figure, the experimental setup is configured in a way to simulate a real small-scale MG. The range of local load variations is also selected in accordance with a real small-scale MG. The proposed control system is implemented on a digital platform using a field-programmable gate array (FPGA).

In order to digitally implement the proposed hybrid observer (shown in Fig. 2), the observer coefficients have been selected such that the stability criteria are satisfied. It should be noted that in digital implementation, the gains of current and voltage sensors and the gains of analogue to digital converters (ADCs) have to be taken into account to select the observer coefficients. The selected values for the coefficients in the digital implementation are listed in Table IV. The presented coefficients are selected to achieve fast and accurate estimation results. As mentioned in Section III, these coefficients are some constant value that does not have to be exact. The proposed observer can reliably operate with different values of parameters as far as they are in the stability range. Therefore, the selected coefficients listed in Table IV do not present the unique tuning result of controller coefficients.

TABLE II
PERFORMANCE OF THE PROPOSED HARMONIC COMPENSATION SYSTEM IN COMPENSATING A WIDE RANGE OF HARMONICS IN COMPARISON WITH THE METHOD PRESENTED IN [34]

	Harmonic Contents Without Compensation		Compensation Percentage	
	Order	Percentage	Voltage Feedback Multi-loop	Proposed Method
Case 1	H3	4.5%	82%	92%
	H5	3%	82%	88%
	H7	3%	80%	87%
Case 2	H3	6%	85%	94%
	H5	6%	85%	91%
	H7	6%	83%	91%
	H9	5%	83%	89%
	H11	5%	83%	87%
Case 3	H3	6%	85%	93%
	H5	6%	85%	91%
	H13	4%	80%	87%
	H21	4%	–	78%
	H29	4%	–	78%
Case 4	H3	5%	82%	90%
	H23	3%	–	74%
	H29	3%	–	74%
	H31	3%	–	71%
	Asynchronous 1495 Hz	2%	–	71%

TABLE III
SPECIFICATIONS OF THE DC/AC CONVERTER EXPERIMENTAL PROTOTYPE

Symbols	Parameters	Values
P_o	Rated Output Power	1 kW
f_{sw}	Switching Frequency	20 kHz
v_{out}	MG Rated Voltage	240 V AC
i_{out}	Rated Output Current	5 A
v_{Bus}	DC-Bus Voltage	400 V DC
L_o	Output Inductor	3.1 mH
C_{Bus}	DC-bus Capacitor	375 μF

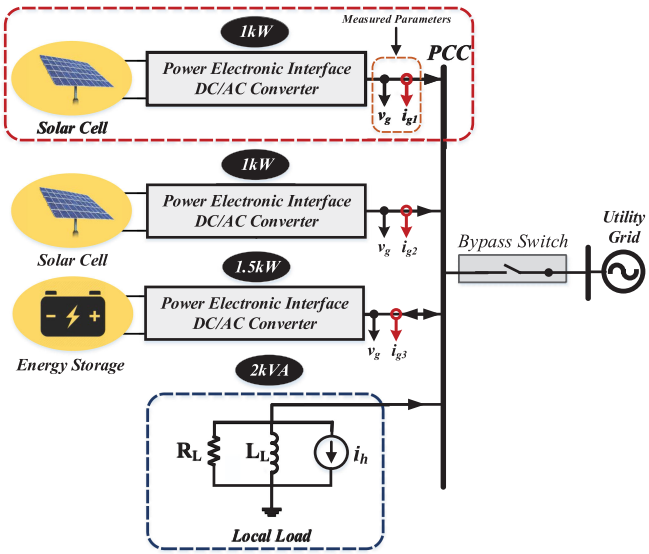

Fig. 12. Configuration of the implemented single-phase MG.

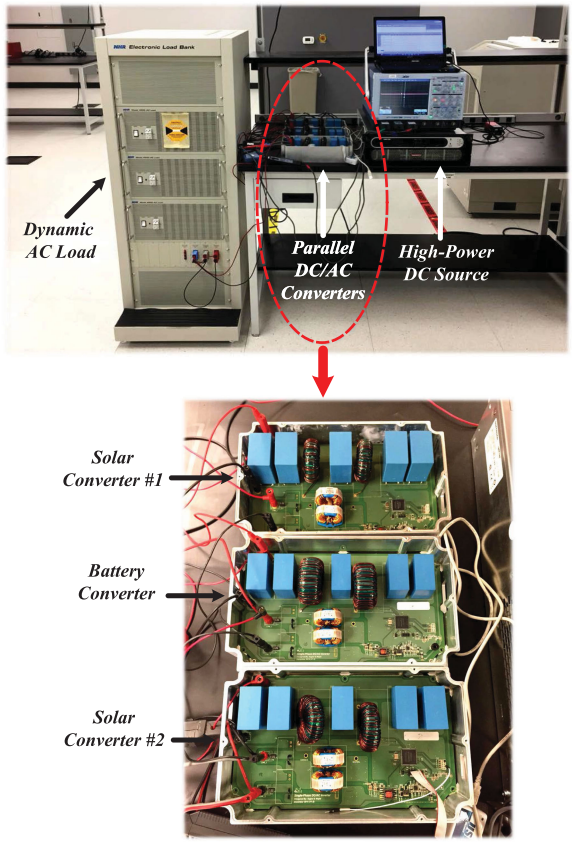

(a)

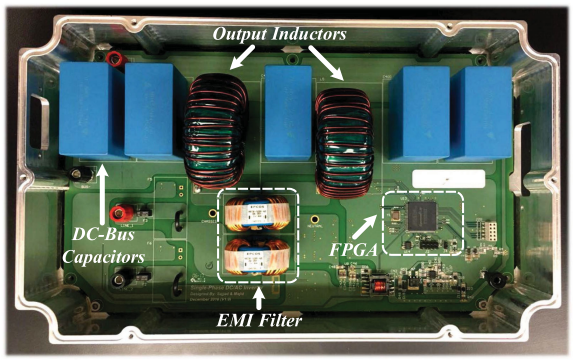

(b)

Fig. 13. MG experimental setup and the experimental prototype of the dc/ac inverter.

TABLE IV
HYBRID LOAD OBSERVER COEFFICIENTS

Symbols	Parameters	Values
μ_{11}, μ_{12}	$\hat{x}_1$ Coefficients	2210
μ_{22}, μ_{21}	$\hat{x}_2$ Coefficients	1730
μ_{33}, μ_{31}	$\hat{x}_3$ Coefficients	3270
γ_1	$\hat{\xi}_1$ Coefficients	3150
γ_2	$\hat{\xi}_3$ Coefficients	52400
γ_3	$\hat{\theta}_1$ Coefficients	56
γ_4	$\hat{\theta}_2$ Coefficients	23100

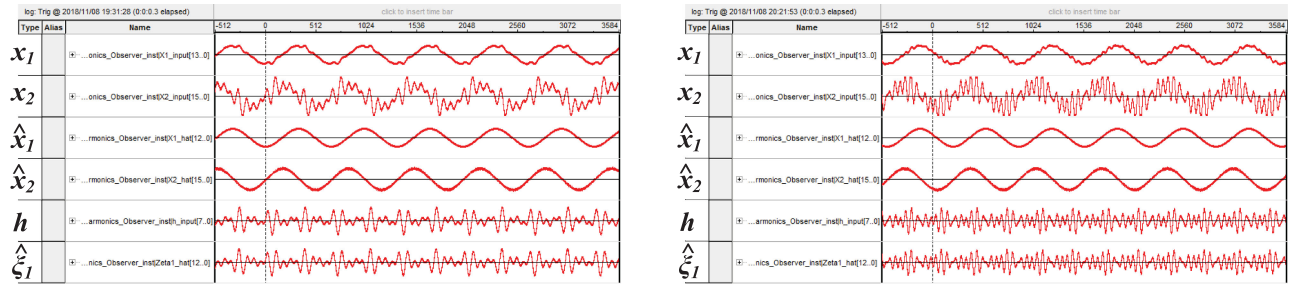

Fig. 14. Real-time signals of digital implementation of the proposed observer in the FPGA, when: (a) 6% fifth harmonic component, a 6% seventh harmonic component, and a 6% ninth harmonic component are applied, and (b) a 6% ninth harmonic component, a 6% eleventh harmonic component, and a 6% thirteenth harmonic component are applied.

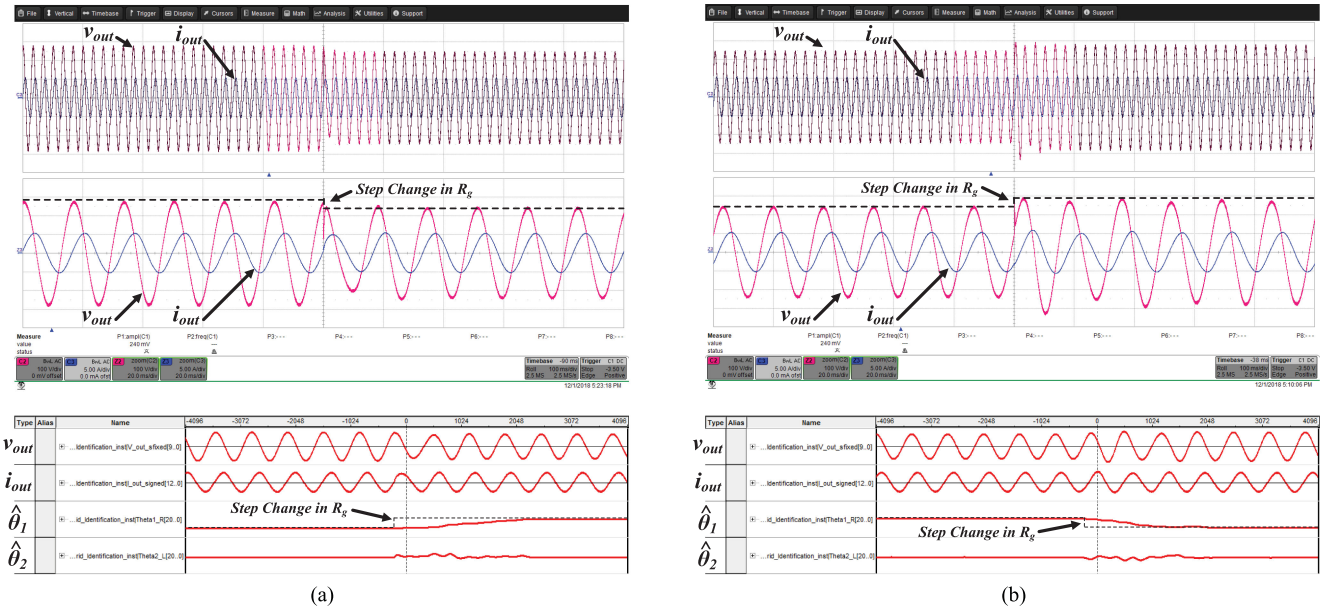

Fig. 15. Transient performance of the proposed hybrid load observer for estimating the linear portion of the load ($\hat{\theta}_1$ and $\hat{\theta}_2$) when: (a) step change of $-200\,\Omega$ is applied to the local load and (b) step change of $200\,\Omega$ is applied to the local load.

Fig. 14 (a) and (b) illustrates various real-time signals obtained from the SignalTap Logic Analyzer of the FPGA. Fig. 14(a) and (b) verifies the capability of the proposed hybrid observer to estimate the exact harmonic contents of the grid voltage in the experimental prototype.

Figs. 15 (a) and (b) and 16(a) and (b) show the transient performance of the hybrid load observer for estimating the linear portion of the local load. These figures show different waveforms such as, the converter output voltage ($v_{\rm out}$), the output current ($i_{\rm out}$), and the real-time signals obtained from the SignalTap (e.g., $v_{\rm out}$, $i_{\rm out}$, $\hat{\theta}_1$, and $\hat{\theta}_2$). In particular, in Fig. 15, the local load resistance has varied from 400 to $200\,\Omega$ in Fig. 15(a) and from 200 to $400\,\Omega$ in Fig. 15(b). In Fig. 16, the local load inductance has varied from 160 to 80 mH in Fig. 16(a) and from 80 to 160 mH in Fig. 16(b). Figs. 15 and 16 verify the capability of the proposed hybrid observer to estimate the exact values of the linear portion of the load as well as precise tracking of load changes in the experimental prototype. It should be noted that Figs. 15 and 16 present the digital values of the estimated load impedance in form of θ_1 and θ_2 ($\theta_1 = 1/R_g$ and $\theta_2 = 1/L_g$). In order to calculate the real values of the load impedance, the gains of current and voltage sensors and the gains of ADCs have to be taken into account.

Fig. 17(a)–(c) shows the transient performance of the proposed control system for compensating the harmonics superimposed on the MG voltage. In order to add the harmonics to the load, a dynamic ac load (shown in Fig. 13) is used in the experimental setup. This load is capable of implementing harmonics up to the thirteenth component. Using this electronic load, a different order of harmonics with different harmonic content percentages can be applied to the MG voltage. Therefore, this electronic load can fairly simulate the disruptive effects of the most of the nonlinear loads connected to MGs. In Fig. 17, a 3% third harmonic component, a 3% fifth harmonic component, and a 3% seventh harmonic component have been superimposed to the MG voltage using the dynamic ac load.

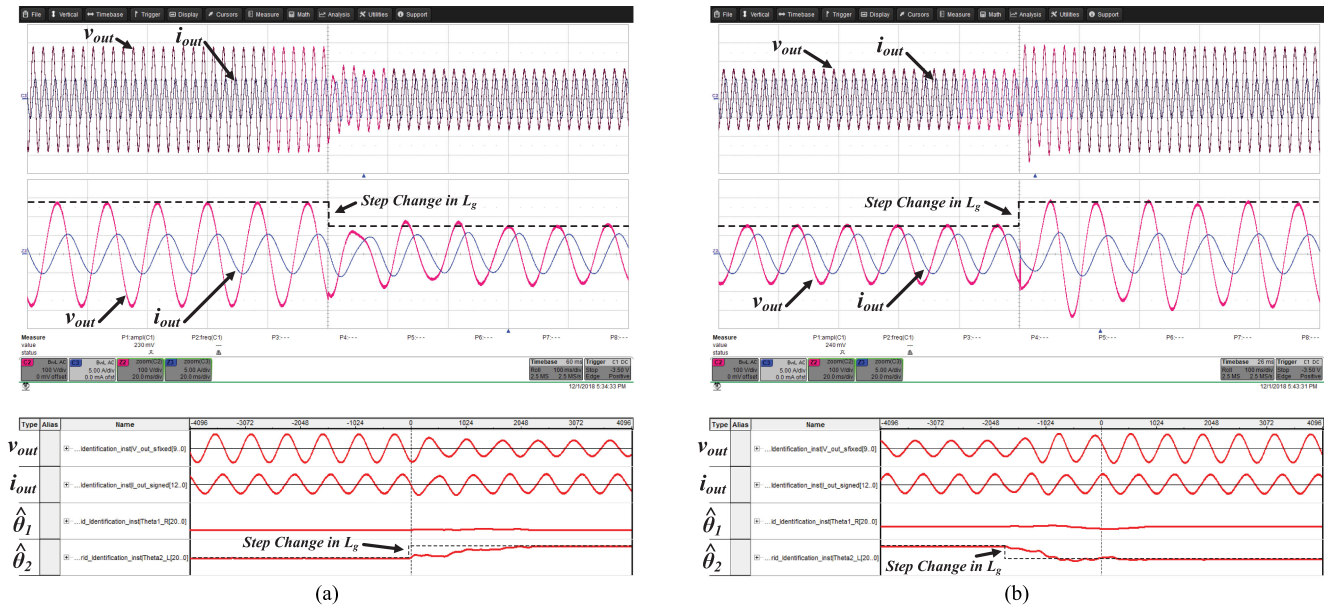

Fig. 16. Transient performance of the proposed hybrid load observer for estimating the linear portion of the load ($\hat{\theta}_1$ and $\hat{\theta}_2$) when: (a) step change of -80 mH is applied to the local load and (b) step change of 80 mH is applied to the local load.

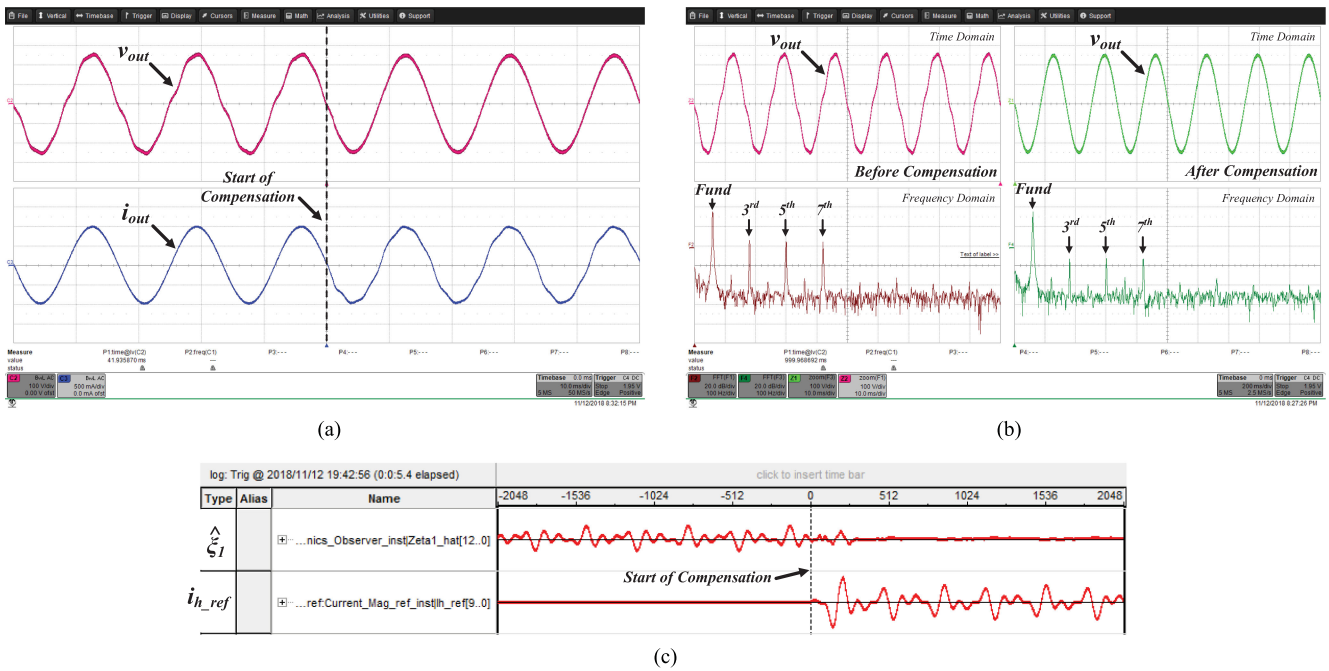

Fig. 17. Transient performance of the proposed control system for compensating the harmonics when a 3% third harmonic component, a 3% fifth harmonic component, and a 3% seventh harmonic component are applied to the MG voltage in (a) time domain, (b) time and frequency domain, and (c) real-time signals of $\hat{\xi}_1$ and $i_{h-\mathrm{ref}}$.

According to Fig. 17(a), when the harmonic compensator is disabled, the harmonic compensation signal $i_{h-\mathrm{ref}}$ is almost zero. In this case, the reference of the current controller is only provided by the fundamental reference generator block that generates a sinusoidal reference signal. Therefore, the converter output current is sinusoidal when the harmonic compensator is disabled. While, according to Fig. 17(a), when the harmonic compensator is enabled, it quickly respond and compensate for harmonics. Fig. 17(b) shows the MG voltage waveform in both frequency and time domains in order to illustrate their harmonic contents. According to Fig. 17(b), the control system could tremendously reduce the voltage harmonics. Fig. 17(c) shows the

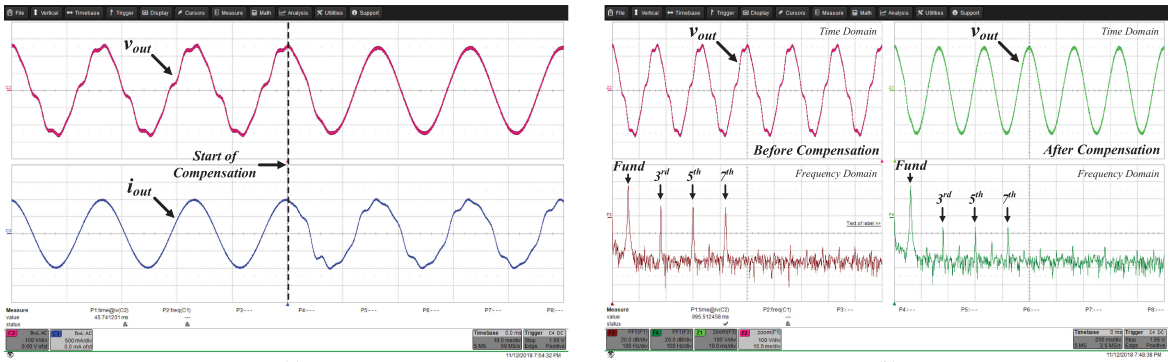

(a) (b)

Fig. 18. Transient performance of the proposed control system for compensating the harmonics when a 6% third harmonic component, a 6% fifth harmonic component, and a 6% seventh harmonic component are applied to the MG voltage in (a) time domain and (b) time and frequency domain.

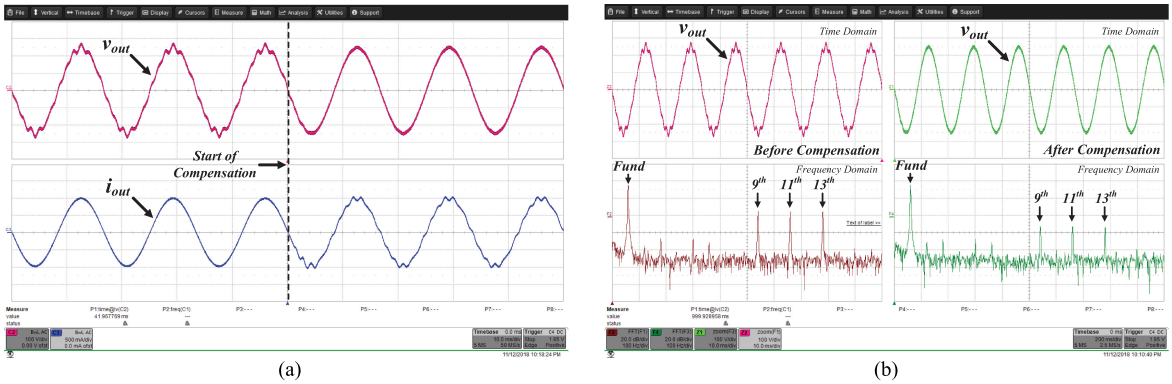

(a) (b)

Fig. 19. Transient performance of the proposed control system for compensating the harmonics when, a 3% ninth harmonic component, a 3% eleventh harmonic component, and a 3% thirteenth harmonic component are applied to the MG voltage in (a) time domain and (b) time and frequency domain.

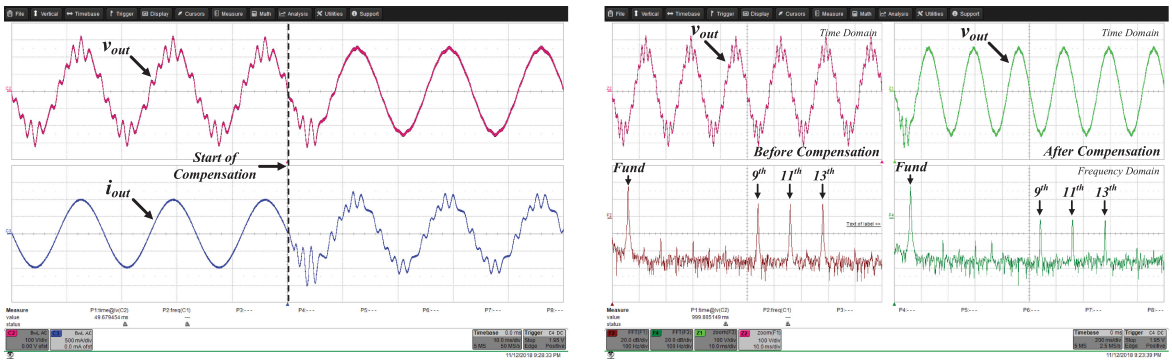

(a) (b)

Fig. 20. Transient performance of the proposed control system for compensating the harmonics when a 10% ninth harmonic component, a 10% eleventh harmonic component, a 10% and thirteenth harmonic component are applied to the MG voltage in (a) time domain and (b) time and frequency domain.

experimental results for harmonics $\hat{\xi}_1$ and the compensation signal $i_{h-\mathrm{ref}}$ from the SignalTap. This figure shows that the proposed harmonic compensator can produce proper reference signal in order to supply the harmonics and in turn highly improve the quality of the voltage.

In order to demonstrate the capability of the presented method in various MG operating conditions, four different cases for different orders and amplitudes of harmonics have been examined. Figs. 18–21 show the transient performance of the proposed control scheme in four different operating conditions. In Fig. 18, a

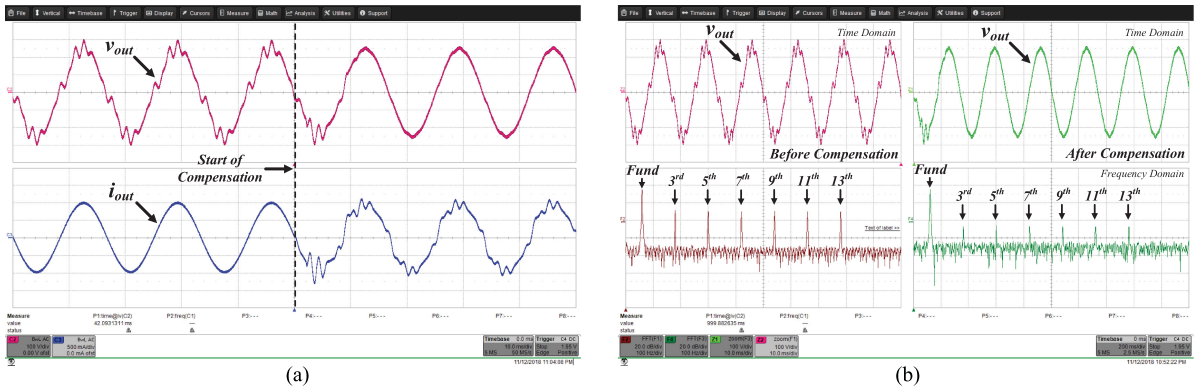

(a) (b)

Fig. 21. Transient performance of the proposed control system for compensating the harmonics when a 6% third harmonic component, a 6% fifth harmonic component, a 6% seventh harmonic component, a 6% ninth harmonic component, a 6% eleventh harmonic component, and a 6% thirteenth harmonic component are applied to the MG voltage in (a) time domain and (b) time and frequency domain.

TABLE V
PERFORMANCE OF THE PROPOSED HARMONIC COMPENSATION SYSTEM IN COMPENSATING THE MG VOLTAGE HARMONICS IN THE EXPERIMENTAL PROTOTYPE

	Harmonic Order	Harmonic Contents (%) Without Compensation	Harmonic Contents (%) Compensation Using the Proposed Method
Case 1	H3	3%	0.27%
	H5	3%	0.265%
	H7	3%	0.3%
	H9	3%	0.31%
	H11	3%	0.415%
	H13	3%	0.45%
Case 2	H3	6%	0.405%
	H5	6%	0.41%
	H7	6%	0.55%
	H9	6%	0.715%
	H11	6%	0.82%
	H13	6%	0.82%

6% third harmonic component, a 6% fifth harmonic component, and a 6% seventh harmonic component have been applied to the MG voltage. According to Fig. 18, the proposed harmonic compensator is able to eliminate the voltage harmonics by supplying load harmonics despite a high amount of load harmonics. Fig. 19 shows the performance of the control system when higher order of harmonics (a 3% ninth harmonic component, a 3% eleventh harmonic component, and a 3% thirteenth harmonic component) have been applied to the MG voltage. This figure shows that the proposed approach is effective for higher order harmonics as well. In order to intensify the impacts of higher order harmonics, a 10% ninth harmonic component, a 10% eleventh harmonic component, and a 10% thirteenth harmonic component have been applied to the load and the results are shown in Fig. 20.

Fig. 21 shows the transient performance in an extreme case where a 6% of third harmonic component, a 6% fifth harmonic component, a 6% seventh harmonic component, a 6% ninth harmonic component, a 6% eleventh harmonic component, and a 6% thirteenth harmonic component have been applied to the MG voltage. According to Fig. 21, even in an extreme condition with a wide range of harmonics, the proposed control system can significantly reduce the MG voltage harmonics.

Table V summarize the results obtained from implementing the proposed harmonic compensation system in the experimental prototype. According to this table, the proposed harmonic compensation system could effectively decrease the harmonic contents of the MG voltage (i.e., compensate for MG load harmonics), by injecting the appropriate harmonic current to the MG.

VIII. CONCLUSION

One of the main challenges with MGs is the harmonics crated by MG nonlinear loads. Dealing with harmonics is particularly challenging in the islanded mode of operation when the harmonics cannot be supplied by the grid. Thus, in the islanded MGs, the control system of the inverters must supply the harmonics in order to have a high quality voltage at the load. In this paper, a new harmonic compensator has been presented, which is able to precisely estimate the harmonic contents and compensate for unknown harmonics. The proposed estimator can extract any types of harmonics/disturbances (synchronous, asynchronous, dc component, etc.). In addition, a hybrid load observer is embedded into the proposed harmonic compensator, which is able to estimate the linear portion of the load in a real-time manner. The proposed control system offers very reliable operation for MGs in the distributed power generation. Simulation and experimental results verify the accuracy and the speed of the proposed control system for estimating and compensating various harmonics.

REFERENCES

[1] F. Blaabjerg, R. Teodorescu, M. Liserre, and A. V. Timbus, "Overview of control and grid synchronization for distributed power generation systems," *IEEE Trans. Ind. Electron.*, vol. 53, no. 5, pp. 1398–1409, Oct. 2006.
[2] A. Abessi, V. Vahidinasab, and M. S. Ghazizadeh, "Centralized support distributed voltage control by using end-users as reactive power support," *IEEE Trans. Smart Grid*, vol. 7, no. 1, pp. 178–188, Jan. 2016.

[3] J. M. Carrasco *et al.* "Power-electronic systems for the grid integration of renewable energy sources: A survey," *IEEE Trans. Ind. Electron.*, vol. 53, no. 4, pp. 1002–1016, Jun. 2006.

[4] K. Yang and A. Walid, "Outage-storage tradeoff in frequency regulation for smart grid with renewables," *IEEE Trans. Smart Grid*, vol. 4, no. 1, pp. 245–252, Mar. 2013.

[5] J. Rocabert, A. Luna, F. Blaabjerg, and P. Rodríguez, "Control of power converters in ac microgrids," *IEEE Trans. Power Electron.*, vol. 27, no. 11, pp. 4734–4749, Nov. 2012.

[6] N. Pogaku, M. Prodanovic, and T. C. Green, "Modeling, analysis and testing of autonomous operation of an inverter-based microgrid," *IEEE Trans. Power Electron.*, vol. 22, no. 2, pp. 613–625, Mar. 2007.

[7] J. M. Guerrero, M. Chandorkar, T. Lee, and P. C. Loh, "Advanced control architectures for intelligent microgrids—Part I: Decentralized and hierarchical control," *IEEE Trans. Ind. Electron.*, vol. 60, no. 4, pp. 1254–1262, Apr. 2013.

[8] M. Prodanovic, K. D. Brabandere, J. V. D. Keybus, T. Green, and J. Driesen, "Harmonic and reactive power compensation as ancillary services in inverter-based distributed generation," *IET Gener., Transmiss. Distrib.*, vol. 1, no. 3, pp. 432–438, May 2007.

[9] F. Tang, J. M. Guerrero, J. C. Vasquez, D. Wu, and L. Meng, "Distributed active synchronization strategy for microgrid seamless reconnection to the grid under unbalance and harmonic distortion," *IEEE Trans. Smart Grid*, vol. 6, no. 6, pp. 2757–2769, Nov. 2015.

[10] M. Hamzeh, H. Karimi, and H. Mokhtari, "Harmonic and negative-sequence current control in an islanded multi-bus MV microgrid," *IEEE Trans. Smart Grid*, vol. 5, no. 1, pp. 167–176, Jan. 2014.

[11] J. He, Y. W. Li, and M. S. Munir, "A flexible harmonic control approach through voltage-controlled DG–grid interfacing converters," *IEEE Trans. Ind. Electron.*, vol. 59, no. 1, pp. 444–455, Jan. 2012.

[12] M. Illindala and G. Venkataramanan, "Frequency/sequence selective filters for power quality improvement in a microgrid," *IEEE Trans. Smart Grid*, vol. 3, no. 4, pp. 2039–2047, Dec. 2012.

[13] R. Teodorescu, F. Blaabjerg, U. Borup, and M. Liserre, "A new control structure for grid-connected LCL PV inverters with zero steady-state error and selective harmonic compensation," in *Proc. 19th Annu. IEEE Appl. Power Electron. Conf. Expo.*, Feb. 2004, vol. 1, pp. 580–586.

[14] M. Liserre, R. Teodorescu, and F. Blaabjerg, "Multiple harmonics control for three-phase grid converter systems with the use of PI-RES current controller in a rotating frame," *IEEE Trans. Power Electron.*, vol. 21, no. 3, pp. 836–841, May 2006.

[15] M. Singh, V. Khadkikar, A. Chandra, and R. K. Varma, "Grid interconnection of renewable energy sources at the distribution level with power-quality improvement features," *IEEE Trans. Power Del.*, vol. 26, no. 1, pp. 307–315, Jan. 2011.

[16] R. Zhao, Q. Li, H. Xu, Y. Wang, and J. M. Guerrero, "Harmonic current suppression strategy for grid-connected PWM converters with LCL filters," *IEEE Access*, vol. 7, pp. 16 264–16 273, 2019.

[17] A. Hamadi, S. Rahmani, and K. Al-Haddad, "A hybrid passive filter configuration for VAR control and harmonic compensation," *IEEE Trans. Ind. Electron.*, vol. 57, no. 7, pp. 2419–2434, Jul. 2010.

[18] W. U. K. Tareen and S. Mekhielf, "Three-phase transformerless shunt active power filter with reduced switch count for harmonic compensation in grid-connected applications," *IEEE Trans. Power Electron.*, vol. 33, no. 6, pp. 4868–4881, Jun. 2018.

[19] Y. Zhang and Y. W. Li, "Grid harmonics compensation using high-power PWM converters based on combination approach," *IEEE J. Emerg. Sel. Topics Power Electron.*, vol. 4, no. 1, pp. 186–197, Mar. 2016.

[20] D. Ahmadi and J. Wang, "Online selective harmonic compensation and power generation with distributed energy resources," *IEEE Trans. Power Electron.*, vol. 29, no. 7, pp. 3738–3747, Jul. 2014.

[21] R. Ni, Y. W. Li, Y. Zhang, N. R. Zargari, and Z. Cheng, "Virtual impedance-based selective harmonic compensation (VI-SHC) PWM for current source rectifiers," *IEEE Trans. Power Electron.*, vol. 29, no. 7, pp. 3346–3356, Jul. 2014.

[22] M. S. Munir, Y. W. Li, and H. Tian, "Improved residential distribution system harmonic compensation scheme using power electronics interfaced DGs," *IEEE Trans. Smart Grid*, vol. 7, no. 3, pp. 1191–1203, May 2016.

[23] A. Micallef, M. Apap, C. Spiteri-Staines, and J. M. Guerrero, "Mitigation of harmonics in grid-connected and islanded microgrids via virtual admittances and impedances," *IEEE Trans. Smart Grid*, vol. 8, no. 2, pp. 651–661, Mar. 2017.

[24] J. He, Y. W. Li, D. Bosnjak, and B. Harris, "Investigation and active damping of multiple resonances in a parallel-inverter-based microgrid," *IEEE Trans. Power Electron.*, vol. 28, no. 1, pp. 234–246, Jan. 2013.

[25] X. Wang, F. Blaabjerg, and P. C. Loh, "Virtual RC damping of LCL-filtered voltage source converters with extended selective harmonic compensation," *IEEE Trans. Power Electron.*, vol. 30, no. 9, pp. 4726–4737, Sep. 2015.

[26] Z. Zeng, H. Yi, H. Zhai, F. Zhuo, and Z. Wang, "Harmonic power sharing and PCC voltage harmonics compensation in islanded microgrids by adopting virtual harmonic impedance method," in *Proc. 43rd Annu. Conf. IEEE Ind. Electron. Soc.*, Oct. 2017, pp. 263–267.

[27] S. Munir and Y. W. Li, "Residential distribution system harmonic compensation using PV interfacing inverter," *IEEE Trans. Smart Grid*, vol. 4, no. 2, pp. 816–827, Jun. 2013.

[28] C. Nie, Y. Wang, W. Lei, M. Chen, and Y. Zhang, "An enhanced control strategy for multiparalleled grid-connected single-phase converters with load harmonic current compensation capability," *IEEE Trans. Ind. Electron.*, vol. 65, no. 7, pp. 5623–5633, Jul. 2018.

[29] Y. W. Li and J. He, "Distribution system harmonic compensation methods: An overview of DG-interfacing inverters," *IEEE Ind. Electron. Mag.*, vol. 8, no. 4, pp. 18–31, Dec. 2014.

[30] J. He, Y. W. Li, and M. S. Munir, "A flexible harmonic control approach through voltage-controlled DG–grid interfacing converters," *IEEE Trans. Ind. Electron.*, vol. 59, no. 1, pp. 444–455, Jan. 2012.

[31] J. He and Y. W. Li, "Hybrid voltage and current control approach for DG-grid interfacing converters with LCL filters," *IEEE Trans. Ind. Electron.*, vol. 60, no. 5, pp. 1797–1809, May 2013.

[32] Z. Zou, Z. Wang, and M. Cheng, "Modeling, analysis, and design of multifunction grid-interfaced inverters with output LCL filter," *IEEE Trans. Power Electron.*, vol. 29, no. 7, pp. 3830–3839, Jul. 2014.

[33] Q. Liu, L. Peng, Y. Kang, S. Tang, D. Wu, and Y. Qi, "A novel design and optimization method of an LCL filter for a shunt active power filter," *IEEE Trans. Ind. Electron.*, vol. 61, no. 8, pp. 4000–4010, Aug. 2014.

[34] X. Zhao *et al.* "A voltage feedback based harmonic compensation strategy for current-controlled converters," *IEEE Trans. Ind. Appl.*, vol. 54, no. 3, pp. 2616–2627, May 2018.

[35] F. Liu, Y. Zhou, S. Duan, J. Yin, B. Liu, and F. Liu, "Parameter design of a two-current-loop controller used in a grid-connected inverter system with LCL filter," *IEEE Trans. Ind. Electron.*, vol. 56, no. 11, pp. 4483–4491, Nov. 2009.

[36] L. Padmavathi and P. A. Janakiraman, "Self-tuned feed-forward compensation for harmonic reduction in single-phase low-voltage inverters," *IEEE Trans. Ind. Electron.*, vol. 58, no. 10, pp. 4753–4762, Oct. 2011.

[37] M. Savaghebi, A. Jalilian, J. C. Vasquez, and J. M. Guerrero, "Secondary control for voltage quality enhancement in microgrids," *IEEE Trans. Smart Grid*, vol. 3, no. 4, pp. 1893–1902, Dec. 2012.

[38] T. S. Abdelgayed, W. G. Morsi, and T. S. Sidhu, "A new harmony search approach for optimal wavelets applied to fault classification," *IEEE Trans. Smart Grid*, vol. 9, no. 2, pp. 521–529, Mar. 2018.

[39] F. Cupertino, E. Lavopa, P. Zanchetta, M. Sumner, and L. Salvatore, "Running DFT-based PLL algorithm for frequency, phase, and amplitude tracking in aircraft electrical systems," *IEEE Trans. Ind. Electron.*, vol. 58, no. 3, pp. 1027–1035, Mar. 2011.

[40] K. Thirumala, M. S. Prasad, T. Jain, and A. C. Umarikar, "Tunable-q wavelet transform and dual multiclass SVM for online automatic detection of power quality disturbances," *IEEE Trans. Smart Grid*, vol. 9, no. 4, pp. 3018–3028, Jul. 2018.

[41] E. A. Feilat, "Detection of voltage envelope using Prony analysis-Hilbert transform method," *IEEE Trans. Power Del.*, vol. 21, no. 4, pp. 2091–2093, Oct. 2006.

[42] C. Chen and Y. Chen, "Comparative study of harmonic and interharmonic estimation methods for stationary and time-varying signals," *IEEE Trans. Ind. Electron.*, vol. 61, no. 1, pp. 397–404, Jan. 2014.

[43] S. K. Jain, P. Jain, and S. N. Singh, "A fast harmonic phasor measurement method for smart grid applications," *IEEE Trans. Smart Grid*, vol. 8, no. 1, pp. 493–502, Jan. 2017.

[44] G. W. Chang, C. Chen, and Y. Teng, "Radial-basis-function-based neural network for harmonic detection," *IEEE Trans. Ind. Electron.*, vol. 57, no. 6, pp. 2171–2179, Jun. 2010.

[45] H. Karimipour and V. Dinavahi, "Extended Kalman filter-based parallel dynamic state estimation," *IEEE Trans. Smart Grid*, vol. 6, no. 3, pp. 1539–1549, May 2015.

[46] J. Qi, K. Sun, J. Wang, and H. Liu, "Dynamic state estimation for multi-machine power system by unscented Kalman filter with enhanced numerical stability," *IEEE Trans. Smart Grid*, vol. 9, no. 2, pp. 1184–1196, Mar. 2018.

[47] M. Nagpal, W. Xu, and J. Sawada, "Harmonic impedance measurement using three-phase transients," *IEEE Trans. Power Del.*, vol. 13, no. 1, pp. 272–277, Jan. 1998.

[48] M. C. D. Piazza, P. Zanchetta, M. Sumner, and D. W. P. Thomas, "Estimation of load impedance in a power system," in *Proc. 9th Int. Conf. Harmon. Quality Power.*, Oct. 2000, vol. 2, pp. 520–525.
[49] L. Asiminoaei, R. Teodorescu, F. Blaabjerg, and U. Borup, "Implementation and test of an online embedded grid impedance estimation technique for PV inverters," *IEEE Trans. Ind. Electron.*, vol. 52, no. 4, pp. 1136–1144, Aug. 2005.
[50] B. Palethorpe, M. Sumner, and D. W. P. Thomas, "System impedance measurement for use with active filter control," in *Proc. 8th Int. Conf. Power Electron. Variable Speed Drives*, Sep. 2000, pp. 24–28.
[51] M. Ciobotaru, R. Teodorescu, P. Rodriguez, A. Timbus, and F. Blaabjerg, "Online grid impedance estimation for single-phase grid-connected systems using PQ variations," in *Proc. IEEE Power Electron. Spec. Conf.*, Jun. 2007, pp. 2306–2312.
[52] V. Salis, A. Costabeber, S. M. Cox, and P. Zanchetta, "Stability assessment of power-converter-based ac systems by LTP theory: Eigenvalue analysis and harmonic impedance estimation," *IEEE J. Emerg. Sel. Topics Power Electron.*, vol. 5, no. 4, pp. 1513–1525, Dec. 2017.
[53] V. Salis, A. Costabeber, P. Zanchetta, and S. Cox, "A generalised harmonic linearisation method for power converters input/output impedance calculation," in *Proc. 18th Eur. Conf. Power Electron. Appl.*, Sep. 2016, pp. 1–7.
[54] H. L. M. Monteiro, M. M. de Oliveira, R. R. Aleixo, C. A. Duque, and P. F. Ribeiro, "A real time implementation of an harmonic impedance estimator," in *Proc. 17th Int. Conf. Harmon. Qual. Power*, Oct. 2016, pp. 333–337.
[55] A. M. Najafabadi and A. T. Alouani, "Real time parameter identification of composite load model," in *Proc. IEEE Power Energy Soc. Gen. Meeting*, Jul. 2013, pp. 1–5.
[56] A. Najafabadi and A. T. Alouani, "Real time estimation of sensitive parameters of composite power system load model," in *Proc. PES Transmiss. Distrib. Conf. Expo.*, May 2012, pp. 1–8.
[57] G. Fusco, A. Losi, and M. Russo, "Constrained least squares methods for parameter tracking of power system steady-state equivalent circuits," *IEEE Trans. Power Del.*, vol. 15, no. 3, pp. 1073–1080, Jul. 2000.
[58] L. Pengfei, T. Shun, Y. Liting, Q. Yeniu, and S. Jian, "An assessment method of power system harmonic impedance based on mixed total least squares," in *Proc. IEEE PES Asia-Pacific Power Energy Eng. Conf.*, Oct. 2016, pp. 1694–1698.
[59] J. C. Vasquez, J. M. Guerrero, A. Luna, P. Rodriguez, and R. Teodorescu, "Adaptive droop control applied to voltage-source inverters operating in grid-connected and islanded modes," *IEEE Trans. Ind. Electron.*, vol. 56, no. 10, pp. 4088–4096, Oct. 2009.
[60] R. Dietz and A. Mertens, "Grid impedance estimation in inductive-resistive distributed power networks using particle filtering," in *Proc. 18th Eur. Conf. Power Electron. Appl.*, Sep. 2016, pp. 1–8.
[61] Z. Xin, X. Wang, P. C. Loh, and F. Blaabjerg, "Realization of digital differentiator using generalized integrator for power converters," *IEEE Trans. Power Electron.*, vol. 30, no. 12, pp. 6520–6523, Dec. 2015.
[62] Y. Tang, P. C. Loh, P. Wang, F. H. Choo, F. Gao, and F. Blaabjerg, "Generalized design of high performance shunt active power filter with output LCL filter," *IEEE Trans. Ind. Electron.*, vol. 59, no. 3, pp. 1443–1452, Mar. 2012.
[63] G. Shen, X. Zhu, J. Zhang, and D. Xu, "A new feedback method for PR current control of LCL-filter-based grid-connected inverter," *IEEE Trans. Ind. Electron.*, vol. 57, no. 6, pp. 2033–2041, Jun. 2010.
[64] R. Teodorescu, F. Blaabjerg, M. Liserre, and P. C. Loh, "Proportional-resonant controllers and filters for grid-connected voltage-source converters," *IEE Proc.—Elect. Power Appl.*, vol. 153, no. 5, pp. 750–762, Sep. 2006.
[65] D. N. Zmood and D. G. Holmes, "Stationary frame current regulation of PWM inverters with zero steady-state error," *IEEE Trans. Power Electron.*, vol. 18, no. 3, pp. 814–822, May 2003.
[66] M. Liserre, R. Teodorescu, and F. Blaabjerg, "Stability of photovoltaic and wind turbine grid-connected inverters for a large set of grid impedance values," *IEEE Trans. Power Electron.*, vol. 21, no. 1, pp. 263–272, Jan. 2006.
[67] S. Eren, M. Pahlevani, A. Bakhshai, and P. Jain, "A digital current control technique for grid-connected AC/DC converters used for energy storage systems," *IEEE Trans. Power Electron.*, vol. 32, no. 5, pp. 3970–3988, May 2017.
[68] S. M. Kaviri, H. Hajebrahimi, M. Pahlevani, P. Jain, and A. Bakhshai, "A hybrid adaptive droop control technique with embedded dc-bus voltage regulation for single-phase microgrids," in *Proc. IEEE Energy Convers. Congr. Expo.*, Oct. 2017, pp. 3359–3366.
[69] S. M. Kaviri, H. Hajebrahimi, M. Pahlevaninejad, P. Jain, and A. Bakhshai, "A new power flow control approach for power converters in single-phase microgrids," in *Proc. IEEE Appl. Power Electron. Conf. Expo.*, Mar. 2018, pp. 1420–1427.
[70] S. Sastry, *Nonlinear Systems: Analysis, Stability, and Control*. Hertfordshire, U.K.: Springer-Verlag, 1999.
[71] A. Arsie and C. Ebenbauer, "Refining Lasalle's invariance principle," in *Proc. Amer. Control Conf.*, Jun. 2009, pp. 108–112.
[72] R. Marino and P. Tomei, *Nonlinear Control Design: Geometric, Adaptive, and Robust*. Hertfordshire, U.K.: Prentice-Hall, 1996.
[73] A. R. Teel, "Asymptotic convergence from L/sub p/ stability," *IEEE Trans. Autom. Control*, vol. 44, no. 11, pp. 2169–2170, Nov. 1999.
[74] A. Khorsandi, M. Ashourloo, and H. Mokhtari, "A decentralized control method for a low-voltage dc microgrid," *IEEE Trans. Energy Convers.*, vol. 29, no. 4, pp. 793–801, Dec. 2014.
[75] U. Akram, M. Khalid, and S. Shafiq, "An improved optimal sizing methodology for future autonomous residential smart power systems," *IEEE Access*, vol. 6, pp. 5986–6000, 2018.
[76] N. Rezaei, A. Ahmadi, A. H. Khazali, and J. M. Guerrero, "Energy and frequency hierarchical management system using information gap decision theory for islanded microgrids," *IEEE Trans. Ind. Electron.*, vol. 65, no. 10, pp. 7921–7932, Oct. 2018.
[77] N. Nikmehr and S. Najafi-Ravadanegh, "Optimal operation of distributed generations in micro-grids under uncertainties in load and renewable power generation using heuristic algorithm," *IET Renewable Power Gener.*, vol. 9, no. 8, pp. 982–990, 2015.

Sajjad Makhdoomi Kaviri (S'14–M'19) received the M.Sc. degree in electrical engineering from the Isfahan University of Technology, Isfahan, Iran, in 2013, and the Ph.D. degree in electrical engineering from Queen's University, Kingston, ON, Canada, in 2019.

His industrial experience includes collaboration with SPARQ systems in developing their highly efficient solar micro-inverter. He has authored 15 journal and conference papers. His research interests include control techniques for dc–dc and ac–dc power converters, micro-grids, and smart grids.

Dr. Kaviri is a member of the IEEE Power and Energy Society.

Majid Pahlevani (S'07–M'12–SM'14) received the Ph.D. degree from Queens University, Kingston, ON, Canada, in 2012.

He is currently an Assistant Professor with the Department of Electrical and Computer Engineering, Queen's University. previously, he was an Assistant Professor with the University of Calgary, Calgary, AB, Canada, from 2016 to 2019. He was also the Chief R&D Engineer, and then, the VP of Technology with SPARQ Systems Inc., from 2011 to 2016. At SPARQ, he invented multiple innovative power circuitry and digital control techniques for SPARQ's main product, QUAD micro-inverter. He collaborated with Freescale Semiconductor Inc., where he was the Leader of a research team working on the design and implementation of the power converters for a pure electric vehicle from 2008 to 2011. He has conducted more than 20 industrial projects in renewable energy systems, energy storage systems, electric vehicles, and LED lighting. He has authored more than 130 journals and conference proceeding papers and is the holder of 40 U.S. patents (issued/pending).

Dr. Pahlevani is the Associate Editor of the IEEE JOURNAL OF EMERGING AND SELECTED TOPICS IN POWER ELECTRONICS and a member of the IEEE Power Electronics Society. He was also the recipient of many awards such as the Early Research Excellence Award from Alberta, Canada, the Engineering and Applied Sciences Outstanding Thesis Award from Queens University, the Research Excellence Award from IEEE Canada, and the Distinguished Research Award from the University of Calgary.

Praveen K. Jain (S'86–M'88–SM'91–F'02) received the M.A.Sc. and Ph.D. degrees in electrical engineering from the University of Toronto, Toronto, ON, Canada, in 1984 and 1987, respectively.

He is a Professor of electrical and computer engineering, a Tier 1 Canada Research Chair in power electronics, and the Director with the Queen's Centre for Energy and Power Electronics Research (ePOWER), Queen's University, Kingston, ON. His 36-year career is marked by significant contributions to the theory and practice of power electronics, and through his considerable work with industry, including Astec, Freescale, General Electric, Intel, and Nortel. In the late 1980s, he played a key role in the design and development of high-frequency power conversion equipment for the International Space Station, Canadian Astronautics. Subsequently, he made pioneering contributions in introducing resonant power conversion technology in telecommunications during his work with Nortel in the 1990s. He is the Founder of two successful start-up companies, CHiL Semiconductor, specializing in digital power solutions (acquired by International Rectifier), and SPARQ Systems, developing innovative photovoltaic micro-inverters. He has supervised and guided almost 100 graduate students, postdoctoral fellows, and power electronics engineers who are well placed in industry and academia. He has authored and coauthored more than 500 papers and holds 93 patents (granted and pending).

Dr. Jain was the recipient of many awards and honors, which include the Queen's Prize for Excellence in Research, the IEEE William Newell Power Electronics Award, the Engineering Medal of the Professional Engineers of Ontario, the IEEE IAS Distinguished Lecturer, a Fellow of the Royal Society of Canada, a Fellow of the Engineering Institute of Canada, and a Fellow of the Canadian Academy of Engineering.

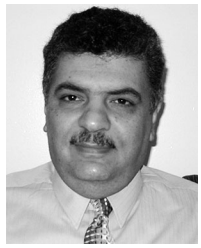

Alireza Bakhshai (M'04–SM'09) received the B.Sc. and M.Sc. degrees from the Isfahan University of Technology, Isfahan, Iran, in 1984 and 1986, respectively, and the Ph.D. degree from Concordia University, Montreal, QC, USA, in 1997.

He is currently a Professor with the Department of Electrical and Computer Engineering, Queen's University, Kingston, ON, Canada. From 1998 to 2004, he was with the faculty of Electrical and Computer Engineering, Isfahan University of Technology. He has acquired 38 international patents (11 granted and 17 pending), and has authored and coauthored more than 50 peer-reviewed journals and more than 100 conference papers in fields including high power electronics and applications, renewable energy conversion, and control systems.

Dr. Bakhshai is a licensed Professional Engineer (PEng) in Ontario.